Cationic Nanohydrogel Particles as Potential siRNA Carriers for Cellular Delivery

Lutz Nuhn,[†] Markus Hirsch,[‡] Bettina Krieg,[‡] Kaloian Koynov,[§] Karl Fischer,[⊥] Manfred Schmidt,[⊥] Mark Helm,[‡] and Rudolf Zentel[†,*]

[†]Institute of Organic Chemistry and [‡]Institute of Pharmacy and Biochemistry, Johannes Gutenberg-University Mainz, Staudingerweg 5, D-55099 Mainz, Germany, [§]Max-Planck-Institute for Polymer Research, Ackermannweg 10, D-55128 Mainz, Germany, and [⊥]Institute of Physical Chemistry, Johannes Gutenberg-University Mainz, Welder Weg 11, D-55021 Mainz, Germany

ABSTRACT Oligonucleotides such as short, double-stranded RNA (siRNA) or plasmid DNA (pDNA) promise high potential in gene therapy. For pharmaceutical application, however, adequate drug carriers are required. Among various concepts progressing in the market or final development, nanosized hydrogel particles may serve as novel transport media especially for siRNA. In this work, a new concept of synthesizing polymeric cationic nanohydrogels was developed, which offers a promising strategy to complex and transport siRNA into cells. For this purpose, amphiphilic reactive ester block copolymers were synthesized by RAFT polymerization of pentafluorophenyl methacrylate as reactive ester monomer together with tri(ethylene glycol)-methyl ether methacrylate. In polar aprotic solvents, a self-assembly of these polymers could be observed leading to the formation of nanometer-sized polymer aggregates. The resulting superstructures were used to convert the reactive precursor block copolymers with amine-containing cross-linker molecules into covalently stabilized hydrogel particles. Detailed dynamic light scattering studies showed that the structure of the self-assembled aggregates can permanently be locked-in by this process. This method offers a new possibility to synthesize precise nanohydrogels of different size starting from various block copolymers. Moreover, *via* reactive ester approach, further functionalities could be attached to the nanoparticle, such as fluorescent dyes, which allowed distinct tracing of the hydrogels during complexation with siRNA or cell uptake experiments. In this respect, cellular uptake of the particles themselves as well as with its payload could be detected successfully. Looking ahead, these novel cationic nanohydrogel particles may serve as a new platform for proper siRNA delivery systems.

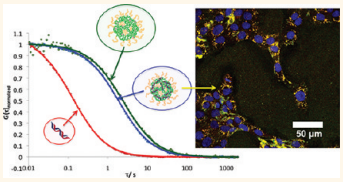

KEYWORDS: nanohydrogel · block copolymer · reactive ester · RAFT polymerization · self-assembled aggregates · siRNA delivery

Nanoscale-sized particles have revolutionized diagnosis and treatment of many diseases within the last decades.[1] Among particles made of various materials, polymeric nanoparticles named nanohydrogels show several advantages for these applications: They are physically or chemically cross-linked hydrophilic polymer networks[2] with a huge loading capacity of water-soluble compounds. They show high stability in physiological media combined with distinct responsiveness to environmental factors. Thus, they have become a promising carrier especially in drug delivery.[3,4] For several years, they have been used as a versatile tool for the delivery of rather advanced drugs like peptides and carbohydrates.[5,6] Even for oligonucleotides, few attempts have been made for the delivery of small interfering RNA (siRNA) using conventionally synthesized nanosized hydrogels.[7−9]

RNA interference (RNAi) itself was discovered by Fire *et al.*[10] and the use of siRNA in mammalian cells by Tuschl *et al.*[11] Due to its ability to knock-down any pathogenic gene, a huge impact of small RNA oligonucleotides for pharmaceutical application was pronounced quickly.[12] However, as most sensible biomacromolecules, double-stranded small RNA molecules are subject to adverse biological interactions such as enzymatic degradation or immune stimulation in biological media. Moreover, because of its highly negatively charged phosphodiester backbone, siRNA is not able to pass important biological barriers, especially the cell membranes, to get to the cytoplasm as its side of action for RNAi. To realize the concept of siRNA as a "magic bullet"[13] in pharmacotherapy, an adequate drug carrier is therefore mandatory for targeted and safe transport, especially after systemic administration.[14]

Several approaches have yet been established during the past decade: While viral vectors are generally seen as highly risky based on their huge immunogenic as well as mutagenic toxicity,[15] research has rather focused on nonviral delivery systems for clinical applications.[16] Small molecules like cationic lipids may offer an opportunity to formulate nanosized lipoplexes for successful siRNA transfection.[17] According to this concept,

* Address correspondence to zentel@uni-mainz.de.

Received for review October 25, 2011 and accepted February 22, 2012.

Published online March 02, 2012
10.1021/nn204116u

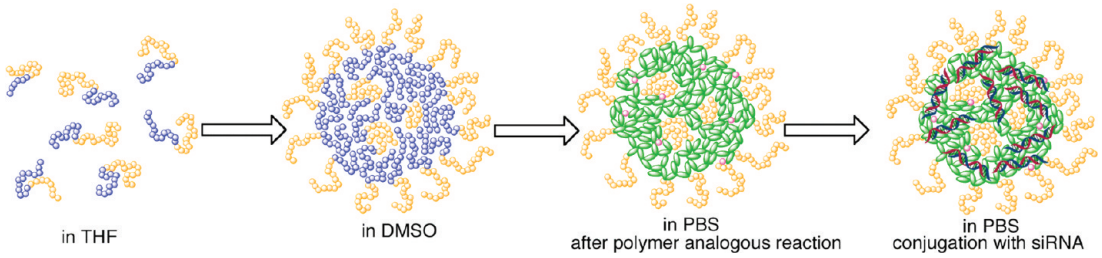

Scheme 1. Synthetic concept of cationic nanohydrogel particles for siRNA transfection.

huge libraries of lipid-like molecules have been synthesized and screened by Anderson *et al.* to find optimal conditions for gene knock-down *in vitro* as well as *in vivo*.[18−21] Overall lipid-based formulations have made so far the biggest progress in current clinical trials of siRNA nanotherapeutics.[22,23]

Alternatively, on the basis of Ringsdorf's concept of polymer therapeutics from the late 1970s,[24,25] several approaches have been established using highly functionalized polymers for siRNA delivery.[26] Both covalent bioconjugates of siRNA and biocompatible polymers as well as noncovalent polyplex formulations with cationic polymers can improve pharmacokinetics and control drug release, as shown for advanced systems recently.[27−30] However, due to controversial concern that modification of siRNA may affect access to enzymatic RNAi protein machinery and thus lead to loss of activity,[31] noncovalent formulations using polycations predominate this area. To reduce their high toxicity, highly functionalized copolymers are needed with biocompatible blocks like PEG[32,33] and HPMA[34] or even responsive[35−38] and targeting elements, too.[39] One of these polymeric systems has recently entered clinical trials successfully and, moreover, could even provide evidence of RNAi in human beings for the first time.[40]

The straightforwardness of both lipoplex as well as polyplex delivery systems is, however, diminished by an aspect rarely taken into account: Their resulting superstructures mainly depend on the polyanionic cargo, namely, the siRNA itself. For example, several techniques developed for transfection of plasmid DNA could not be transferred as transport vehicles for siRNA easily due to the big discrepancy of the oligonucleotides' molecular weight.[41] Taking into account siRNA's molecular weight of about 14 kDa, it is too small to ensure charge-derived stability of a nanosized particle in contrast to plasmid DNA. In addition, the aggregation formation from various siRNAs may differ, as well. Moreover, further competitive interaction with several polyanionic compounds of any biological environment (*e.g.*, albumin) might be possible. Consequently, the dynamics in the system's superstructure may weaken strong electrostatic interactions between delivering vehicle and its payload. Furthermore, additional interference can be caused by extreme dilution with high ionic strength solvents especially after systemic administration. In this respect, it will almost be impossible to adjust pharmacokinetics because of differences in the lipoplex or polyplex structure. Above all, this may possibly limit further clinical use of these systems.[42]

Instead, it is important to have precise nanoparticular delivery systems that are able to transport siRNA and at the same time show stable physical properties in size and shape independent from their payload or any further dynamic interference. Taking all of these concerns into account, nanohydrogels[2−4] may become a perfect tool for siRNA delivery. They are predefined in size and shape and can therefore guarantee safe delivery especially *in vivo*. For example, Siegwart *et al.* recently synthesized libraries of cationic core−shell nanoparticles containing a large variety of hydrophilic shell structures as well as secondary or tertiary amine cross-linkers, which even allow successful siRNA *in vivo* transfection to liver hepatocytes.[43]

On the basis of these results, we have established a new technique of synthesizing cationic nanohydrogel particles with a precise understanding of nanoparticle formation and siRNA loading. Using well-defined amphiphilic reactive ester precursor polymers with an aggregation tendency in polar aprotic solvents like dimethyl sulfoxide, we demonstrate a new tool for generating covalently stabilized hydrogel superstructures by cross-linking the hydrophobic reactive inner core with amine-containing cross-linker molecules (Scheme 1). The physical properties of the resulting nanoparticles can be described carefully before and after conjugation with siRNA, and moreover, the loaded particles show proper cell uptake.

RESULTS AND DISCUSSION

In this work, we synthesized polymeric nanohydrogel particles containing cationic cores for stable conjugation of siRNA and cellular delivery of this sensitive biological material. For this approach, we developed the concept of using amphiphilic reactive ester block copolymers for nanoparticle synthesis. Due to their aggregation behavior in polar solvents, the block copolymers' resulting superstructures can be applied as precursors for final nanoparticle formation (Scheme 1).

We used the reversible addition−fragmentation chain transfer (RAFT) polymerization technique[44,45] to

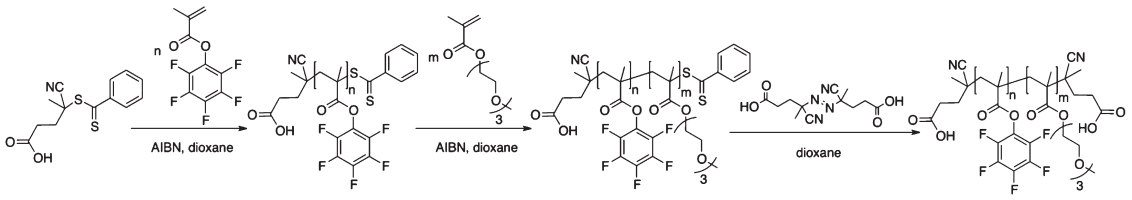

Scheme 2. RAFT block copolymerization of P(PFPMA)-*b*-P(MEO_3MA).

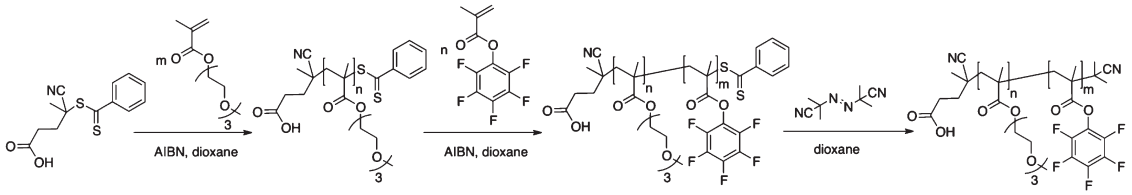

Scheme 3. RAFT block copolymerization of P(MEO_3MA)-*b*-P(PFPMA).

TABLE 1. P(PFPMA)-*b*-P(MEO_3MA) Block Copolymers

	mono/macroCTA/AIBN	*t* (h)	*p* (%)	M_{cal} (g/mol)	DP[c]	M_n[d] (g/mol)	M_w[d] (g/mol)	PDI[d]
$P(PFPMA)_{61}$-*b*-$P(MEO_3MA)_{26}$	100:1:0.1	14	62[a]	30000	26	21600	25900	1.20
$P(PFPMA)_{59}$-*b*-$P(MEO_3MA)_{40}$	150:1:0.1	88	33[b]	26600	40	24500	27700	1.13
$P(PFPMA)_{59}$-*b*-$P(MEO_3MA)_{40}$	150:1:0.1	18	27[b]	24500	40	24500	27700	1.13
$P(PFPMA)_{70}$-*b*-$P(MEO_3MA)_{33}$	140:1:0.1	90	29[b]	27400	33	25800	29400	1.14

[a] Conversion determined gravimetrically. [b] Conversion determined by ^{1}H NMR. [c] Degree of polymerization. [d] M_n, M_w, and PDI determined by GPC.

TABLE 2. P(MEO_3MA)-*b*-P(PFPMA) Block Copolymers

	mono/macroCTA/AIBN	*t* (h)	*p* (%)	M_{cal} (g/mol)	DP[c]	M_n[d] (g/mol)	M_w[d] (g/mol)	PDI[d]
$P(MEO_3MA)_{12}$-*b*-$P(PFPMA)_{25}$	40:1:0.1	88	66[b]	9900	25	9600	11800	1.23
$P(MEO_3MA)_{44}$-*b*-$P(PFPMA)_8$	40:1:0.1	20	56[a]	16200	8	12600	14600	1.16
$P(MEO_3MA)_{46}$-*b*-$P(PFPMA)_{20}$	50:1:0.1	90	60[b]	18600	20	16000	18100	1.13
$P(MEO_3MA)_{49}$-*b*-$P(PFPMA)_{52}$	100:1:0.1	90	64[b]	27800	52	24800	28700	1.16
$P(MEO_3MA)_{46}$-*b*-$P(PFPMA)_{115}$	200:1:0.1	110	67[b]	44800	115	39900	48700	1.22

[a] Conversion determined gravimetrically. [b] Conversion determined by ^{1}H NMR. [c] Degree of polymerization. [d] M_n, M_w, and PDI determined by GPC.

synthesize well-defined block copolymers. As one of the monomers, we chose pentafluorophenyl methacrylate (PFPMA) as the strongly hydrophobic moiety, which is at the same time sensitive toward primary amines preferentially.[46,47] It is compatible with RAFT polymerization[46,48] and allows complete conversion to functional biocompatible polymers after polymer analogous reaction.[49−51] On the other hand, we chose tri(ethylene glycol)methyl ether methacrylate (MEO_3MA) as hydrophilic monomer. It is one of the shortest oligoethylene oxide methacrylate monomers having a LCST considerably above body temperature.[52] At the same time, it has a biocompatibility comparable to PEG with all its advantages for pharmaceutical application.[46,53−55] Both monomers[46,52] as well as 4-cyano-4-(phenylcarbonothioylthio)pentanoic acid[56] as chain transfer agent for RAFT polymerization could be synthesized successfully (Supporting Information) and were used for homo- and block copolymerization. We decided to synthesize the block copolymers in two ways starting from either a PFPMA or MEO_3MA block. As seen from Table S1 (Supporting Information), we were able to polymerize PFPMA, yielding polymers with PDIs below 1.29 and molecular weight in the range of 11.8 to 18.0 kg/mol. Alternatively, we polymerized MEO_3MA first, too. Again, we could vary molecular weight between 3.2 and 11.7 kg/mol but obtained smaller PDIs below 1.23 (Supporting Information Table S2).

Both types of homopolymers could be used in additional RAFT polymerization as macrochain transfer agent. Consequently, we generated block copolymers of either P(PFPMA)-*b*-P(MEO_3MA) or P(MEO_3MA)-*b*-P(PFPMA) composition. Afterward, the dithiobenzoate end group was removed according to Perrier *et al.*[57] to avoid interference during polymer analogous reaction with amines[58] as well as objectionable toxicity.[59] To maintain the block's polarity, we used AIBN for removing dithiobenzoate at the P(PFPMA) end block and ACVA containing a polar carboxyl acid group for P(MEO_3MA) (Scheme 2 and Scheme 3). In this way, the

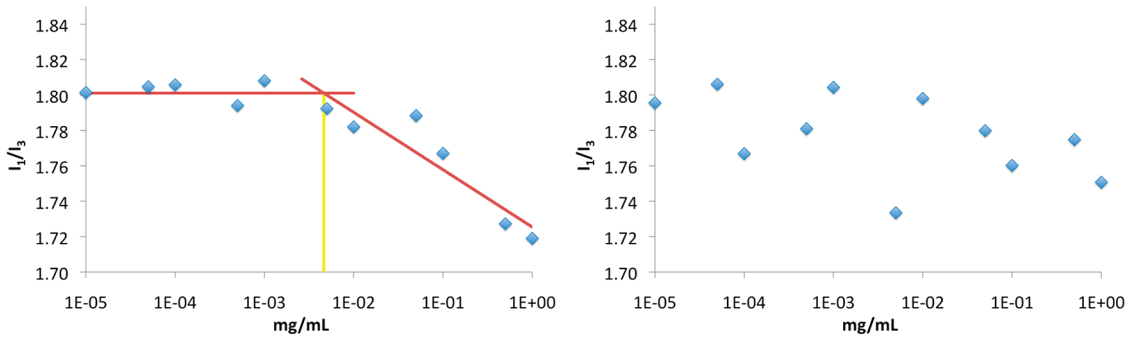

Figure 1. Critical aggregation concentration (CAC) estimation using pyrene fluorescence spectroscopy (relative intensity proportion of first vibronic band at 372 nm to third vibronic band at 385 nm) for various concentrations of $P(PFPMA)_{61}$-*b*-$P(MEO_3MA)_{26}$ (left) and $P(MEO_3MA)_{44}$-*b*-$P(PFPMA)_8$ (right).

block copolymers collected in Table 1 and Table 2 were prepared: those with composition of P(PFPFMA)-*b*-P-(MEO_3MA) had molecular weights between 25.9 and 29.4 kg/mol and PDIs below 1.20. They usually contained 60−70 mol % of hydrophobic units (Table 1). As for block copolymers with $P(MEO_3MA)$-*b*-P(PFPFMA) sequence, we were able to vary the molecular weights in the range between 9.6 and 48.7 kg/mol while keeping the PDIs below 1.23. The majority of these polymers contained again 50−70 mol % of PFPMA units, while two candidates had a higher MEO_3MA block ratio: $P(MEO_3MA)_{46}$-*b*-$P(PFPFMA)_{20}$ contained 30 mol % of PFPMA units and $P(MEO_3MA)_{44}$-*b*-$P(PFPFMA)_8$ had only 15 mol % of hydrophobic units (Table 2).

The aggregation tendency of the block copolymers was investigated because this property is necessary for nanoparticle formation. However, water as a common solvent for amphiphilic polymers could not be used in our case because it would promote base-catalyzed hydrolysis of the reactive ester. Thus, nonaqueous solvents with high polarity had to be used instead. Fortunately, partially fluorinated block copolymers can phase separate in organic solvents such as MeOH, EtOH, DMF, and DMSO.[60,61] Due to its low toxicity, we chose DMSO and looked for a critical aggregation concentration (CAC) by pyrene fluorescence spectroscopy.[62−64] Exemplary, $P(PFPMA)_{61}$-*b*-$P(MEO_3MA)_{26}$ with a block copolymer composition of 70 mol % of perfluorated units showed a clear CAC of 5 μg/mL. In contrast to this, for $P(MEO_3MA)_{44}$-*b*-$P(PFPMA)_8$ with only 15 mol % of hydrophobic units, a CAC was not clearly detectable (Figure 1). Therefore, only those polymers having small polar portions with minor sterical hindrance for aggregation and a rather large fluorinated block contributing to the hydrophobic effect were logically chosen for nanoparticle synthesis.

Having a closer look at $P(PFPMA)_{61}$-*b*-$P(MEO_3MA)_{26}$ with its CAC at 5 μg/mL, we used dynamic light scattering (DLS) to study its solubility in THF and DMSO. THF, which is a good solvent for fluorinated polymers, was selected as solvent to study the nonaggregated state (we also performed GPC analysis of the polymers in THF). Because of carboxylic acid functionalities on the polymer end groups, light scattering experiments had to be done in the presence of 0.01 M LiBr for shielding charge-based interaction between the polymers. Even so, it was rather challenging to detect unimolecularly solubilized polymers in THF. The data obtained with LiBr are indicative of mostly polymer unimers with a negligible portion of small aggregates resulting in an average hydrodynamic radius of about 6 nm. This is still too large for randomly coiled polymers of a molecular weight of 21.6 kg/mol but nevertheless much smaller than without the addition of LiBr. On the contrary, light scattering data from DMSO showed clear aggregate formation of $P(PFPMA)_{61}$-*b*-$P(MEO_3MA)_{26}$ both at 2 and 0.2 mg/mL far above CAC (Figure 2, Table 3). In contrast to THF as solvent, the formation of these aggregates in DMSO was independent of the addition of LiBr (Supporting Information Figure S5, Figure S6, and Table S3). Polymer−DMSO formulations were prepared by simply dissolving the solid polymers supported by sonication for about 1 h. The clear solutions we obtained from this procedure were used for either light scattering or nanohydrogel synthesis. Besides, we also dissolved polymers in THF as a good solvent followed by slowly adding 20% DMSO. Afterward, we removed THF *via* vacuum evaporation at 10 mbar for 24 h. The aggregates resulting from this advanced method were again analyzed by DLS and did not show any significant difference compared to samples prepared by simple dissolving supported by sonication (Figure 3). All aggregates prepared from $P(PFPMA)_{61}$-*b*-$P(MEO_3MA)_{26}$ in DMSO usually showed a hydrodynamic radius of about 50 nm by DLS (Table 3), which is higher than expected for a defined block copolymer micelle. Thus, the resulting superstructure can be expected to have a rather complex aggregate structure comparable to a compound micelle (Scheme 1).[65−67]

The preorganized aggregates were used as novel precursors for synthesizing polymeric nanoparticles *via* amine-based cross-linking of the aggregated reactive ester block copolymers. As cross-linking moiety, we chose spermine, an endogenously produced oligoamine[68] with two primary and two secondary

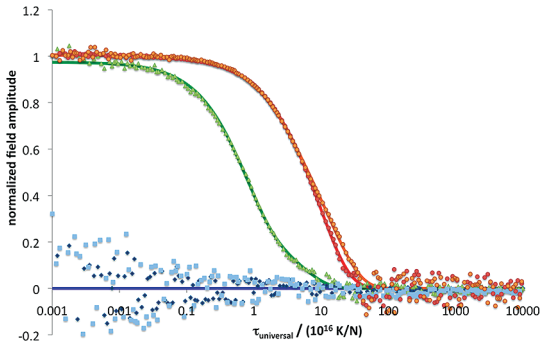

Figure 2. DLS autocorrelation at 30° (raw data points and corresponding fit function) of $P(PFPMA)_{61}$-*b*-$P(MEO_3MA)_{26}$: blue, blank solvent (dark, THF; light, DMSO); green, 1 mg/mL in THF 0.01 M LiBr; red, 2 mg/mL in DMSO 0.01 M LiBr; orange, 0.2 mg/mL in DMSO prepared by THF solvent exchange. To normalize solvent-derived differences in decay times τ due to solvent-specific viscosity η, refractive index n, and scattering vector $q = (4\pi \cdot n/\lambda)\sin(\theta/2)$, we calculated $\tau_{universal}$ as $\tau_{universal} = \tau(q^2 \cdot T/\eta)$.

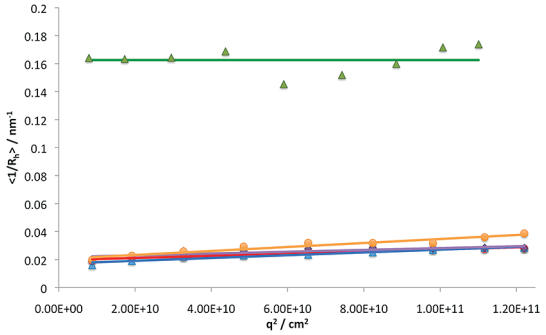

Figure 3. DLS angle dependency of $\langle 1/R_h \rangle$ (raw data points and corresponding extrapolation function) of $P(PFPMA)_{61}$-*b*-$P(MEO_3MA)_{26}$: green, 1 mg/mL in THF (0.01 M LiBr); blue, 2 mg/mL in DMSO; red, 2 g/L in DMSO (0.01 M LiBr); violet, 0.2 mg/mL in DMSO; orange, 0.2 mg/mL in DMSO prepared by THF solvent exchange.

amines. We generally used 0.5 equiv of spermine per 1 equiv of PFPMA unit to adjust cross-linking as well as conjugation for oligonucleotides: while spermine's primary amines may preferably react with pentafluorophenyl esters forming cross-linking amide bonds,[46] the two secondary amines, mostly protonated at physiological pH, can offer a conjugation moiety for siRNA with its negatively charged phosphodiester backbone. Besides, polymer spermine derivatives have already been used for siRNA transfection successfully according to literature.[69−71] Moreover, the reactive ester approach offers several advantages for nanoparticle synthesis because further functionalities can additionally be attached to the particle. For example, we chose a fluorescent dye (Oregon Green cadaverine) to label particles for cell uptake or fluorescent correlation spectroscopy. As previously reported, conversion of fluorinated reactive ester polymers can easily be followed by ^{19}F NMR.[72,73] We used this strategy to detect PFPMA conversion or cross-linking over time and were able to determine complete conversion by this technique (Supporting Information Figure S7). After ^{19}F NMR did not show polymer-bound pentafluorophenol any more (polymer bound signals at −150.3 to −151.39 ppm (br, 2F, o-Ar*F*), −156.91 ppm (br, 1F, p-Ar*F*), and −162.05 ppm (br, 2F, m-Ar*0*); free pentafluorophenolat −168.28 ppm (d, 2F, o-Ar*F*), −168.58 ppm (t, 2F, M-Ar*F*), and −183.39 ppm (t, 2F, p-Ar*0*), Supporting Information Figure S7), cross-linking of the aggregate was complete. However, additional methoxy triethylene glycol amine was added to remove final traces of polymer-bound toxic pentafluorophenol, whose signals might be below the resolution of ^{19}F NMR.[74] After additional time for final reactive ester conversion, the resulting nanohydrogel particles were purified by dialysis against water for several days to remove all small molecular byproducts. Importantly, no free toxic pentafluorophenol could be detected by ^{19}F NMR in the purified samples (Supporting Information Figure S7). They could be stored after subsequent lyophilization as dry powder and could be resuspended in water or buffer (Scheme 4). In Table 4, all nanohydrogel particles prepared by this procedure are collected. **NP1**−**NP7** were prepared from various block copolymers following the same procedure, while for **NP1***−**NP3***, we added, in addition, a small amount of Oregon Green cadaverine. For instance, $P(PFPMA)_{61}$-*b*-$P(MEO_3MA)_{26}$ as the precursor polymer was used for both **NP1** and **NP1*** (Table 4).

The size of the covalently cross-linked nanohydrogel particles was determined by various methods. Dynamic light scattering could be done with particles, which were not fluorescently labeled. We prepared three different solutions of **NP1** in PBS independently (two of 0.1 mg/mL and one 0.01 mg/mL). Each sample gave a hydrodynamic radius of about 50 nm (Figure 4), which is in good aggrement with the size of the precursor aggregates of $P(PFPMA)_{61}$-*b*-$P(MEO_3MA)_{26}$ in DMSO. Thus, the cross-linking of the aggregates

TABLE 3. DLS Results of $P(PFPMA)_{61}$-*b*-$P(MEO_3MA)_{26}$ under Various Conditions

	M_n (g/mol)	solvent	$R_h = \langle 1/R_h \rangle_Z^{-1}$ (nm)	μ_2
$P(PFPMA)_{61}$-*b*-$P(MEO_3MA)_{26}$	21600	1 mg/mL THF, 0.01 M LiBr	6.15	not applicable
		2 mg/mL DMSO	58.47	0.07
		2 mg/mL DMSO, 0.01 M LiBr	51.04	0.08
		0.2 mg/mL DMSO	46.04	0.07
		0.2 mg/mL DMSO (prepared from THF)	48.94	0.07

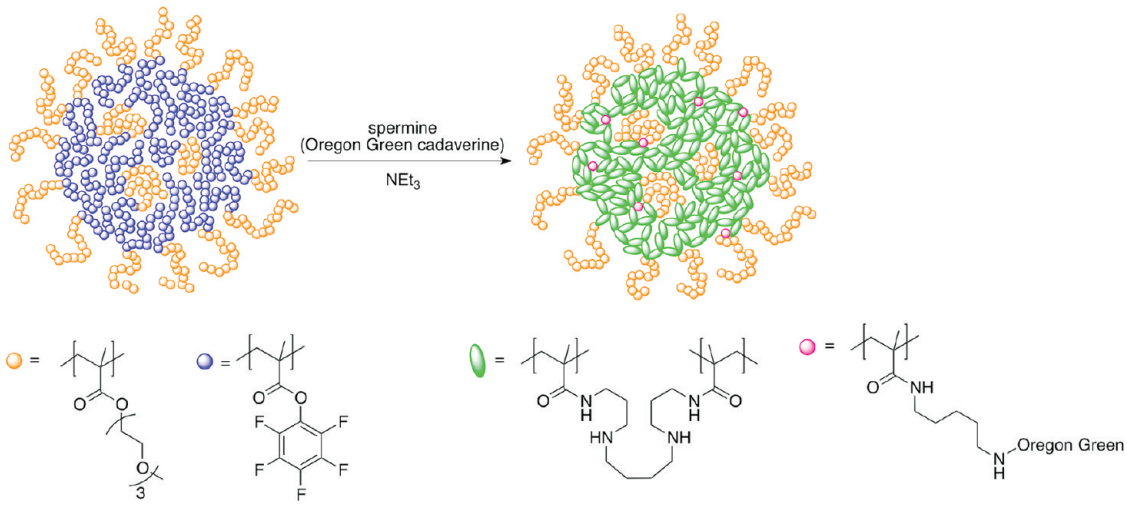

Scheme 4. Nanohydrogel particle synthesis.

TABLE 4. Nanohydrogel Particle Synthesis[a]

	polymer	M_n (g/mol)	equiv of spermine per PFPMA	equiv of fluorescent dye per PFPMA	equiv of triethylamine per PFPMA	reaction time for complete conversion (h)	sequential addition of equiv of methoxy triethylene glycol amine per PFPMA	additional reaction time (h)
NP1	$P(PFPMA)_{61}$-*b*-$P(MEO_3MA)_{26}$	21600	0.500		6.0	16	0.8	24
NP2	$P(MEO_3MA)_{46}$-*b*-$P(PFPMA)_{20}$	16000	0.500		6.0	16	0.8	24
NP3	$P(MEO_3MA)_{46}$-*b*-$P(PFPMA)_{115}$	39000	0.500		6.0	16	0.8	24
NP4	$P(MEO_3MA)_{49}$-*b*-$P(PFPMA)_{52}$	24800	0.500		6.0	19	1.0	20
NP5	$P(MEO_3MA)_{12}$-*b*-$P(PFPMA)_{25}$	9600	0.500		6.0	19	1.0	20
NP6	$P(PFPMA)_{70}$-*b*-$P(MEO_3MA)_{33}$	25800	0.500		6.0	19	1.0	20
NP7	$P(PFPMA)_{59}$-*b*-$P(MEO_3MA)_{40}$	24500	0.500		6.0	19	1.0	20
NP1*	$P(PFPMA)_{61}$-*b*-$P(MEO_3MA)_{26}$	21600	0.500	0.001	6.0	16	1.0	20
NP2*	$P(MEO_3MA)_{46}$-*b*-$P(PFPMA)_{20}$	16,000	0.500	0.001	6.0	16	0.8	24
NP3*	$P(MEO_3MA)_{46}$-*b*-$P(PFPMA)_{115}$	39,000	0.500	0.001	6.0	16	1.0	20

[a] Reaction time for complete conversion was determined by ^{19}F NMR (Supporting Information Figure S7).

seems to conserve the structure during nanoparticle synthesis.

To study the influence of the copolymers' structure on the aggregation and the resulting nanohydrogel conformation, DLS measurements of further nanohydrogel particles were performed. Figure 5 and Table 5 show the results of these measurements: all polymers used for **NP1**, **NP3**, or **NP5** synthesis had a similar block copolymer composition or hydrophilic to hydrophobic ratio of about 30 mol % of MEO_3MA and 70 mol % of PFPMA but varied in their molecular mass. The resulting nanohydrogel particles had different hydrodynamic radii in PBS that increase with the molecular weight of the precursor block copolymers (Supporting Information Table S4 and Figure S8): increasing the molecular weight by a factor of 4 results in a hydrodynamic radius that is 2 times bigger. Thus, we believe that within the given range we are able to adjust the size of the final particle by choosing the molecular weight of the starting block copolymer. Moreover, the μ_2 values obtained by cumulant fitting at 90° of the DLS measurements of **NP1**, **NP3**, and **NP5** were always of similar value (Table 3 and Table 5). Consequently, we assume that consistent polymer composition results in similar aggregate structure and similar hydrogel conformation without any increase in polydispersity.

In addition, the behavior of **NP2** differed from other particles, as we used $P(MEO_3MA)_{46}$-*b*-$P(PFPMA)_{20}$ as precursor polymer: it consists of only 30 mol % of perfluorated units combined with a relatively large hydrophilic part. The resulting nanohydrogel particle **NP2** showed a reasonable average hydrodynamic radius; however, $\langle 1/R_h \rangle$ had a higher angle dependency and the μ_2 value was rather large compared to all other measurements (Figure 5 and Table 5). As we could already show for $P(MEO_3MA)_{44}$-*b*-$P(PFPMA)_8$ with only 15 mol % of hydrophobic units, no CAC was detectable by pyrene fluorescence spectroscopy. Increasing the hydrophobic part to about 30 mol % in $P(MEO_3MA)_{46}$-*b*-$P(PFPMA)_{20}$, as used for **NP2**, may result in aggregation in DMSO, but due to large polar block copolymer portions with sterical hindrance and only minor

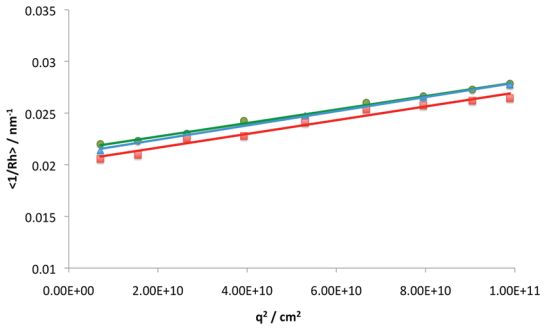

Figure 4. DLS angle dependency of $\langle 1/R_h \rangle$ (raw data points and corresponding extrapolation function) of NP1: green and blue, 0.1 mg/mL NP1 in PBS prepared independently; red, 0.01 mg/mL NP1 in PBS.

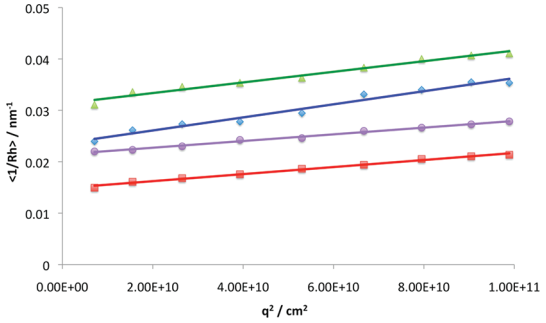

Figure 5. DLS angle dependency of $\langle 1/R_h \rangle$ (raw data points and corresponding extrapolation function) of hydrogel particles in PBS 0.1 mg/mL: violet, NP1; blue, NP2; red, NP3; green, NP5.

nonpolar compositions for hydrophobic interaction, these aggregates might be rather flexible and less stable. The resulting nanohydrogels, therefore, show higher polydispersities.

AFM imaging of the particles was performed to characterize nanohydrogel size individually. Therefore, the nanoparticles were dispersed in water, dripped on mica, and dried in vacuum. The resulting samples were imaged by constant amplitude tapping mode (intermittent contact mode) in air. According to their inner covalently cross-linked core, their structure could be preserved during the preparation process. Small particles with diameters in the range of about 80−150 nm could be visualized (Figure 6). For **NP1**, **NP3**, and **NP5**, their size was in rough agreement with the results obtained by DLS, and they showed fairly homogeneous distributions, too. In contrast to this, **NP2** was again rather polydisperse. High-resolution AFM images showed small as well as larger particles that were not as spherical as those obtained for other particles. These results may again explain the rather large μ_2 value for **NP2** obtained by DLS. Consequently, the concept of high hydrophilic proportions in the precursor polymers destabilizing aggregation formation can be proven again. Looking at the particles' height profiles, they showed only 10% of the diameter obtained by DLS. Taking into account that DLS was done in an aqueous environment, the hydrogel particles are probably swollen, which may later contribute to effective drug loading. During the preparation process for AFM imaging, solvent inside the nanohydrogel gets lost. This may lead to a flattening of the particles onto the substrate as detected by the AFM tip during the scanning process (Figure 6).

According to these results, we were interested in the swelling behavior of the nanoparticle. While AFM sample preparation only allows us to image the nanoparticles attached to a surface, DLS enables us to characterize it in various solvents. Depending on the solution properties, swelling can be influenced, affording different hydrodynamic radii. Thus, we performed additional DLS experiments and varied the solvents for nanoparticle **NP1**. First, we changed the ionic strength by diluting a stock solution of **NP1** with aqueous sodium chloride resulting in 10, 100, and 1000 mM NaCl. However, no difference was observed, as seen from both the autocorrelation function at 30° and the angle dependency of $\langle 1/R_h \rangle$ (Supporting Information Figure S9, Figure S10, and Table S5). We assume that a certain concentration of ions is always present in our hydrogel. A variation in ionic strength inside the nanoparticle is probably smaller than in the surrounding solution during the experiments we performed. In addition, the nanohydrogel particles are highly cross-linked as a consequence of their synthesis (stiochiometric ratio of primary amines and reactive esters). Thus, the osmotic forces are not strong enough to induce significant expansion or shrinkage of the network. In contrast to this, an increase in size was detected when changing the pH of the buffered solvent. Under physiological conditions at pH 7.4, as observed by dispersing **NP1** in PBS, we usually measured an average hydrodynamic radius of about 50 nm. However, lowering the pH using sodium acetate (NaOAc) buffer at pH 4.5, a shift to larger decay times

TABLE 5. DLS Results for Nanohydrogel Particles

		polymer	M_n (g/mol)	ratio hydrophilic/hydrophobic	$R_h = \langle 1/R_h \rangle_Z^{-1}$ (nm)	μ_2
	0.1 mg/mL PBS				47.15	0.08
NP1	0.1 mg/mL PBS, repeated	$P(PFPMA)_{61}$-*b*-$P(MEO_3MA)_{26}$	21600	3:7	47.50	0.07
	0.01 mg/mL PBS				49.21	0.08
NP2	0.1 mg/mL PBS	$P(MEO_3MA)_{46}$-*b*-$P(PFPMA)_{20}$	16000	7:3	42.48	0.11
NP3	0.1 mg/mL PBS	$P(MEO_3MA)_{46}$-*b*-$P(PFPMA)_{115}$	39000	3:7	67.32	0.05
NP5	0.1 mg/mL PBS	$P(MEO_3MA)_{12}$-*b*-$P(PFPMA)_{25}$	9600	3:7	31.96	0.07

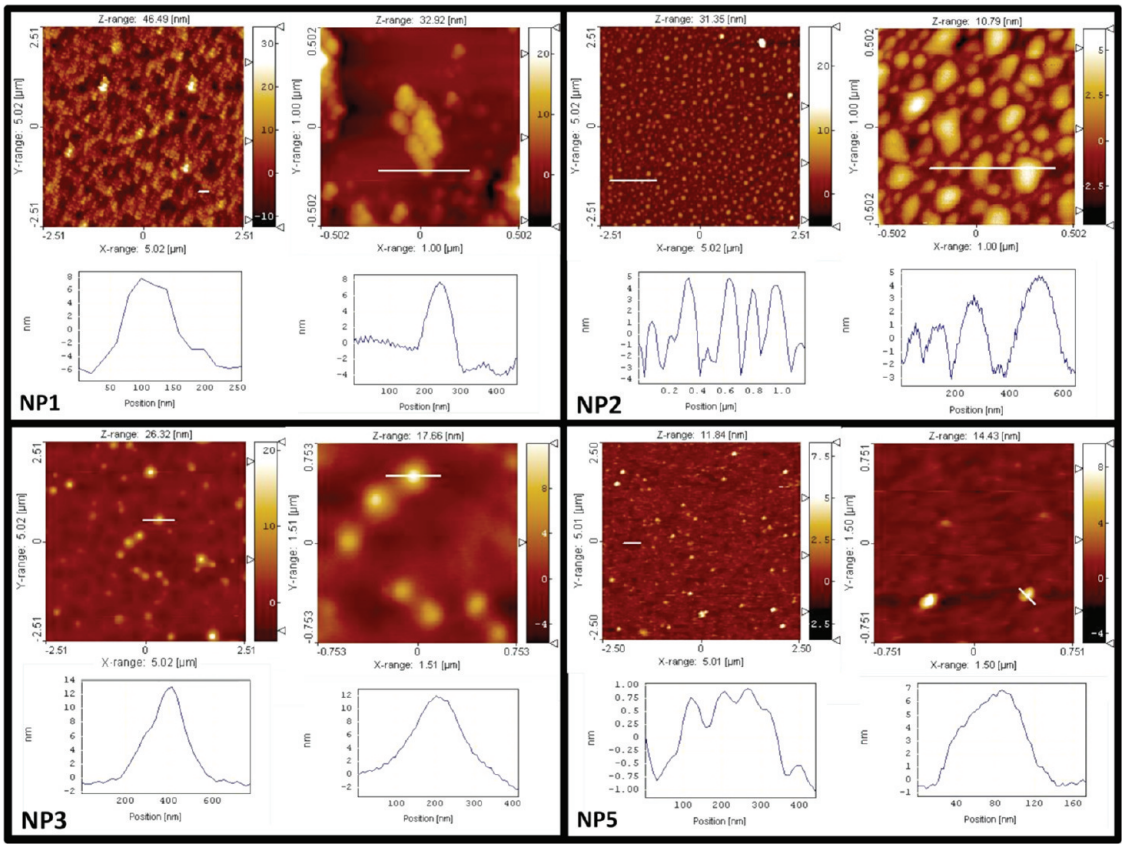

Figure 6. AFM images with height profiles (white bars inside the images) of nanohydrogel particles.

could be detected by the autocorrelation function at 30° (Figure 7). Analyzing the angle dependencies of $\langle 1/R_h \rangle$, we obtained average hydrodynamic radii for **NP1** at pH 4.5 of about 55 nm, which is about 10% bigger than the results in PBS at pH 7.4 (Figure 8, Table 6). The swelling of the nanohydrogel is probably caused by a higher degree protonation of the spermine moieties inside the particles. According to literature data, the pK_a values of the two secondary amines are about 8.85 and 7.96, thus very close the pH value of PBS.[75] Consequently, not all secondary amines inside the particle are completely protonated in PBS. In NaOAc buffer, however, an increasing charge repulsion inside the nanohydrogel may afford stronger forces that are able to expand the network.

Nanohydrogel particles, which were fluorescently labeled with Oregon Green cadaverine during their synthesis, could not be characterized by DLS using a laser at 514.5 nm. In this case, fluorescence correlation spectroscopy (FCS) offers another versatile technique to determine the particle diffusion coefficient or hydrodynamic radius. Exemplary, **NP1***, which was made from the same polymer P(MEO_3MA)$_{46}$-*b*-P($PFPMA$)$_{20}$ like **NP1**, was analyzed. Its R_h determined by FCS was again about 50 nm (Figure 10 and Table 7) and thus in good agreement with the results of the light scattering experiments. Consequently, nanoparticle synthesis in the presence of a small fraction of fluorescent dye does not interfere with the system and can therefore be used as a useful tool for nanohydrogel labeling.

The nanohydrogel's capacity to transport siRNA was determined in PBS buffer at physiological pH 7.4. For a simple gel electrophoresis experiment at optimum detection limit, 210 ng of Atto590-labeled siRNA was mixed with 2.1, 5.25, 10.5, or 21.5 μg of **NP1*** and incubated for 30 min. Afterward, the mixtures were analyzed and separated into the components by gel electrophoresis on a 0.5% agarose gel at 90 V for 50 min and visualized by imaging with a conventional hand-held digital camera upon excitation at 365 nm. Due to their fluorescent labels, siRNA molecules were detectable by red fluorescent light while the hydrogel particles emitted a green light. Mixed colors resulting from an overlay of emission from both dyes were in evidence. At a weight to weight ratio of 25:1 **NP1***/siRNA, hardly any free siRNA was detectable. All siRNA was entrapped by the nanohydrogel particles and kept inside the nanohydrogel (Figure 9). This ratio could be calculated into a secondary amine to phosphodiester ratio of N/P = 30 (compare Supporting Information, calculation of N/P ratio). Obviously, total charge compensation between the two components could not be achieved. As already shown by the DLS experiments, total protonation of all secondary amines at pH 7.4 may not be given completely, since the pK_a values of spermine's secondary amines are close to the pH of PBS. Additionally, charge repulsion inside

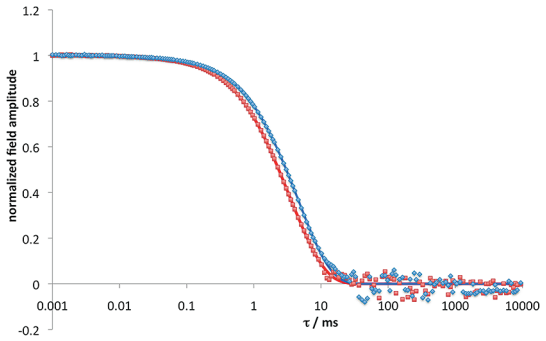

Figure 7. DLS autocorrelation at 30° (raw data points and corresponding fit function) of NP1 0.025 mg/mL in buffer at various pH: red, PBS buffer pH 7.4; blue, NaOAc buffer pH 4.5.

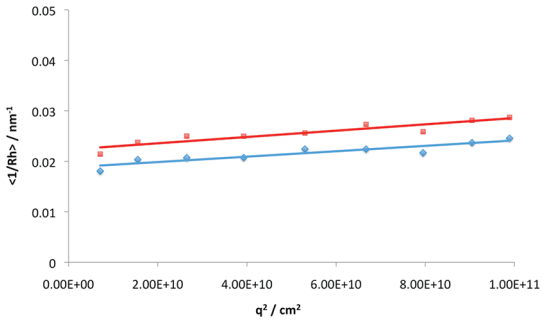

Figure 8. DLS angle dependency of $\langle 1/R_h \rangle$ (raw data points and corresponding extrapolation function) of NP1 0.025 mg/mL in buffer at various pH: red, PBS buffer pH 7.4; blue, NaOAc buffer pH 4.5.

TABLE 6. DLS Results of NP1 in Buffers at Various pH

		$R_h = \langle 1/R_h \rangle_Z^{-1}$ (nm)	μ_2
NP1	0.025 mg/mL in PBS buffer pH 7.4	47.16	0.07
	0.025 mg/mL in NaOAc buffer pH 4.5	55.65	0.08

the highly cross-linked network may reduce the ability of each secondary amine to be protonated, as well. Furthermore, strong sterical hindrance inside the network prevents the polyanionic siRNA from accumulating in the core of the nanogel excessively. This may explain the obtained N/P ratio for this system in Figure 9. Nonetheless, the nanohydrogels show a notable capacity to conjugate siRNA at physiological pH that is mostly driven by charge interaction between the two components.

The nanohydrogel's ability to conjugate with siRNA could also be observed on the nanoscale level performing FCS measurement. To determine the fluorescently labeled particles' hydrodynamic radii alone, we used an argon laser emitting at 488 nm for exciting Oregon Green molecules covalently attached to the nanohydrogel. For tracing siRNA molecules, we chose fluorescent dyes that can be excited at longer wavelengths to exclude interference with the nanoparticles' fluorescence. Therefore, we chose Atto590-labeled siRNA with an excitation maximum around 590 nm. As for **NP1***, we

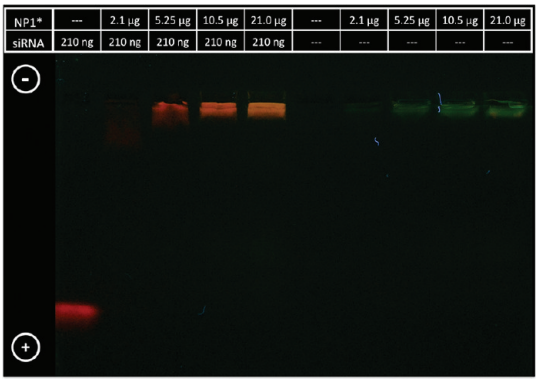

Figure 9. Agarose gel (0.5%) electrophoresis at 90 V for 50 min of various weight to weight ratios of NP1* (green) to siRNA (red) as indicated in the panel in the upper part of the image. The orientation of the electric field is indicated by symbols of the plus and minus poles.

checked carefully that its fluorescent properties did not interfere with Atto590. The FCS setup provides a helium–neon laser emitting at 543 nm, where no fluorescence autocorrelation could be detected for **NP1*** alone. Additionally, we did fluorescence spectroscopy to verify this for the ensemble average of **NP1***, too (Supporting Information Figure S11). Consequently, we were able to measure the autocorrelation of freely diffusing siRNA as well as the siRNA's autocorrelation in presence of **NP1*** using the helium–neon laser for excitation at 543 nm.

The results confirmed again efficient loading of the nanohydrogel particle with siRNA. Measurements of siRNA alone allowed us to determine a hydrodynamic radius of about 2.3 nm for this double-stranded oligonucleotide. However, when siRNA was mixed with **NP1*** at a weight to weight ratio of 80:1 **NP1***/siRNA, the autocorrelation function of the resulting fluorescence fluctuation was quantitatively shifted to higher decay times (Figure 10). In agreement with the previous gel electrophoresis experiment, the FCS data confirm that siRNA was completely associated with the nanohydrogel particles. The resulting autocorrelation function could nicely be fitted by a single component fit (*i.e.*, $m = 1$), yielding a diffusion time τ_D of about 1900 μs or on an average hydrodynamic radius of about 33 nm (Table 7). The size of **NP1*** alone, however, determined at 488 nm excitation, was about 50 nm and hence in good agreement with the results of the light scattering experiments for **NP1**. Thus, the particle's stable shape was not really affected by loading with siRNA. The accuracy of the FCS data was not good enough to clearly quantify the observed shrinkage. Nonetheless, siRNA incorporation into the nanohydrogel particles could lead to some reduction in their hydrodynamic radius, which may result from electrostatic interaction between the phosphodiester groups of the siRNA with the protonated amine species. Consequently, charge-based repulsion among the protonated amines would be

TABLE 7. FCS Results of NP1* (Determined with Argon Laser at 488 nm) and siRNA Alone and with NP1* (Determined with Helium Neon Laser at 543 nm)

		τ_D (μs)	R_h (nm)
NP1*	36 μg/mL PBS	2429.6 ± 34.4	53.1 ± 2.4
siRNA	0.28 μg/mL PBS	129.6 ± 0.8	2.3 ± 0.1
siRNA + **NP1***	307 μL **NP1*** (36 μg/mL PBS) + 20 μL siRNA (7 μg/mL PBS)	1898.6 ± 14.5	33.3 ± 1.9

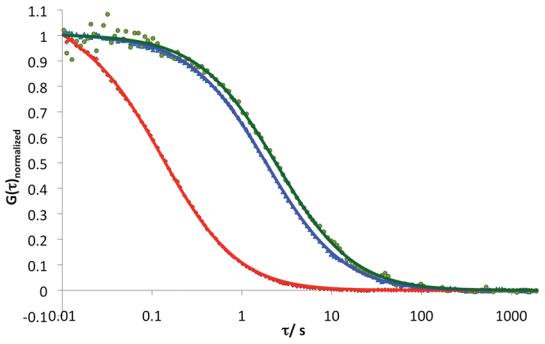

Figure 10. FCS autocorrelation curve of Atto590-labeled siRNA alone (red symbols) and in the presence of NP1* (blue symbols) at 80:1 weight to weight ratio of NP1* to siRNA (excitation at 543 nm). NP1* alone (green symbols) (excitation at488 nm). The solid lines represent the corresponding singe component fits (m = 1).

neutralized. Summing up, these results proved again that the vast majority of siRNA can successfully be conjugated into the cationic nanohydrogel and does not affect the nanoparticular shape of its transport vehicle significantly (Scheme 5).

The final question to be answered is whether the new nanohydrogel particles can be taken up by cells alone as well as with siRNA as their payload. Thus, we incubated RBE4 cells for 4 and 24 h with **NP1*** alone, siRNA alone, or with particles loaded with the maximum amount of siRNA (weight ratio of 25:1 **NP1***/siRNA, according to the gel electrophoresis experiments we performed before). Afterward, we observed cellular uptake *via* confocal laser scanning microscopy. On the basis of their orthogonal fluorescent functionalization, the cell's nuclei (stained with DAPI), **NP1***, and siRNA could be imaged independently.

NP1* alone showed direct cellular uptake, which was carefully confirmed by z-stack analysis (Supporting Information Figure S12). The hydrogel particles were detected in small vesicular spots in close vicinities around the nuclei, suggesting endocytotic uptake inside the cells. Moreover, comparing 4 and 24 h incubation time, a strong increase of uptake was visualized based on increasing green fluorescence signals inside the cells after 24 h (Figure 11 and Figure 12). To exclude nonspecific uptake of siRNA, we incubated the cells with Atto590-labeled siRNA alone for 4 h. However, we did not observe any siRNA-derived fluorescence inside the cells. Only incubation of siRNA with commercially available cationic lipids like Oligofectamine showed

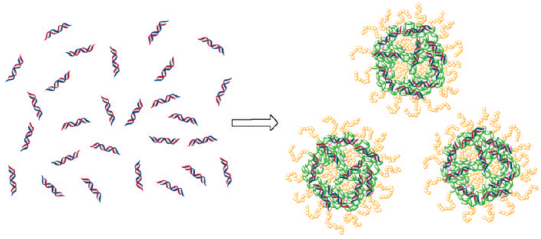

Scheme 5. Nanohydrogel particles conjugated with siRNA.

siRNA uptake within the same time frame (Figure 11). Consequently, this cell line requires a transfection reagent for siRNA uptake.

Thereafter, incubation of siRNA together with nanohydrogel particles could be performed. We looked at both Oregon Green labeled particles **NP1*** with unlabeled siRNA (Figure 11 and Figure 12) as well as unlabeled particles **NP1** with Atto590-labeled siRNA (Supporting Information Figure S13) and could always detect labeled compounds inside the cells. Finally, both labeled siRNA and **NP1*** were observed after 4 and 24 h incubation. For both experiments, a colocalization of **NP1*** with siRNA was found when looking at channels of detected fluorescence derived from each laser excitation independently: those vesicular spots containing **NP1*** excited at 488 nm could also be visualized by excitation at 561 nm, where Atto590-labeled siRNA emits its fluorescence, suggesting colocalization of siRNA and **NP1*** inside the cell. Moreover, comparing 4 and 24 h incubation time, an increase of uptake was again visualized based on strong fluorescence signals for both compounds inside the cells after 24 h (Figure 11 and Figure 12).

Consequently, these experiments ensure that RBE4 cells can both uptake nanohydrogel particles alone and nanohydrogel particles conjugated with siRNA effectively. Over time, an increase of uptake can be visualized, too. However, ongoing experiments have not yet shown sufficient knock-down efficiency of the particles loaded with siRNA within similar incubation periods of the cell uptake studies. Taking into account the nanohydrogel particles' physical properties, there is no trigger inside that may induce vast release of their payload after cellular uptake into the cytoplasm. With DLS measurements, we could determine certain responsiveness to different pH levels resulting in a change in size of the nanohydrogel particle. In this respect, a certain degree of buffering capacity might be given by residual nonprotonated secondary amine moieties inside the nanoparticle. They may contribute to an osmotic swelling

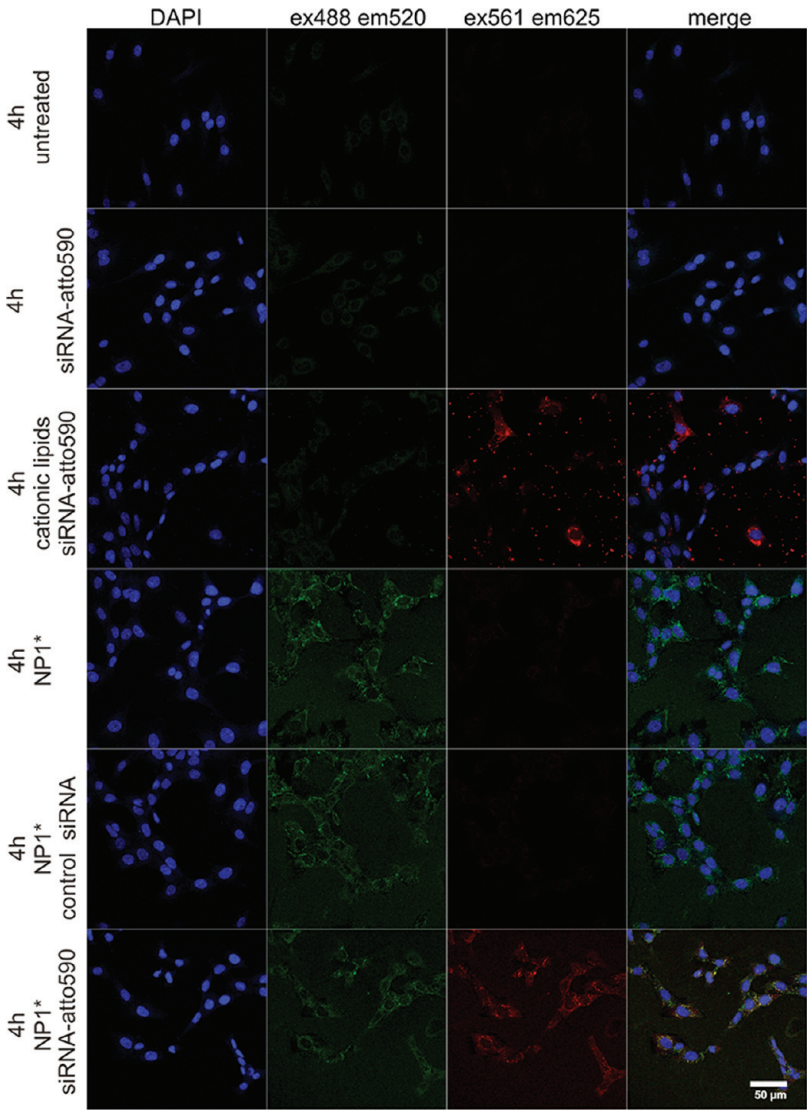

Figure 11. Fluorescent confocal microscopy images of RBE4 cells untreated or incubated for 4 h with siRNA alone or with Oligofectamine, NP1* alone, or with unlabeled or Atto590-labeled siRNA; NP1* labeled with Oregon Green (green), nuclei stained with DAPI (blue), and siRNA is unlabeled or Atto590 labeled (red).

of the endosome resulting in eventual release into the cytosol.[76] Afterward, the transported siRNA would need to get access to the RNAi enzyme machinery, which could only be achieved effectively by release from the nanohydrogel particle. In our case, this could only be realized by nonspecific replacement with other cytoplasmic given polyanionic components like mRNA or anionic peptides. Since the alignment of this equilibrium inside the cell is probably a long-lasting process, we were not able to observe sufficient knock-down efficiency within the incubation period of the cell uptake studies.

An alternative perspective contributing to effective siRNA knock-down is currently under evaluation by using stimuli-responsive cross-linked nanohydrogel particles. A stronger responsiveness to a change of pH or reduction potential, which can occur after cellular uptake, would further promote degradability of the nanoparticle. This would also include better access of the particles' payload to the RNAi machinery. However, these aspects are not yet given by the system presented in this work. Nonetheless, we soon expect effective delivery using degradable systems regarding the delivery of oligonucleotides (siRNA and pDNA) *in vitro*. This would also promote *in vivo* application, where biodegradability is mandatory to avoid nanoparticle accumulation.

CONCLUSION

In this work, we present a novel technique for a controlled synthesis of polymeric nanoparticles as cationic nanohydrogels for siRNA complexation. We used the RAFT polymerization technique to synthesize well-defined amphiphilic reactive ester block copolymers of P(PFPMA)-*b*-P(MEO_3MA) and P(MEO_3MA)-*b*-P(PFPMA). We found an aggregation tendency for these polymers in polar aprotic solvents like dimethyl sulfoxide. The resulting superstructures could be used as precursors

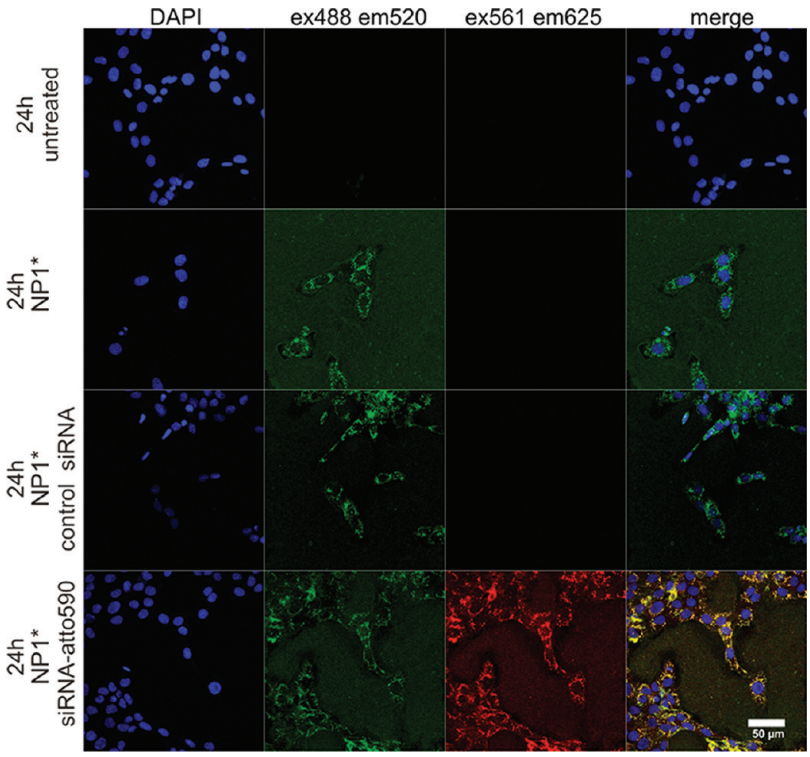

Figure 12. Fluorescent confocal microscopy images of RBE4 cells untreated or incubated for 24 h with siRNA alone, NP1* alone, or with unlabeled or Atto590 labeled siRNA; NP1* labeled with Oregon Green (green), nuclei stained with DAPI (blue), and siRNA is unlabeled or Atto590 labeled (red).

to generate covalently stabilized nanohydrogel particles by cross-linking the hydrophobic reactive inner core with amine-containing cross-linker molecules. Spermine could be used as a cross-linker when adjusted stoichiometrically to half of all PFPMA units, providing additional functionalities for conjugation with siRNA. After purification, the final nanogels could be lyophilized, stored as dry powder, and resuspended for further use. Dynamic light scattering before and after cross-linking revealed preservation of the aggregate's structure. Moreover, when using block copolymers of similar block ratio but different molecular weight, we were able to adjust the size of the resulting nanohydrogels. Both DLS and AFM could confirm that less stable precursor aggregates containing block copolymers with a higher hydrophilic ratio led to polydisperse cross-linked nanoparticles. Lowering the pH by dispersing the particles from PBS to NaOAc buffer led to a 10% swelling of the hydrodynamic radius. Adding an amine-functionalized fluorescent dye during hydrogel synthesis, however, did not affect the system as determined by FCS and AFM. The labeled particles could therefore be used for tracing conjugation between siRNA and particle as well as in cell uptake studies. With agarose gel electrophoresis, we saw complete complexation compensation of nanoparticle to siRNA at a 25:1 weight to weight ratio. FCS was a versatile tool to verify the complexation of siRNA to the particle on a nanoscale level, too. Significant influence on the nanoparticle's shape and solution properties could be neglected. Thus, compared to other polyplex systems, the resulting superstructure of siRNA and our delivering vehicle does not mainly depend on the payload but can be adjusted beforehand during particle synthesis. To this respect, our concept enables the use of well-defined nanohydrogels as universal carriers for a variety of siRNAs with adjustable size and shape properties. Finally, we saw proper time-dependent uptake of these particles alone as well as loaded with siRNA. Ongoing experiments using stimuli-responsive cross-linkers for triggered release of the payload after cell uptake will test the efficiency of this system to stimulate gene-specific knock-down caused by the nanoparticles' payload. Consequently, we propose promising advantages of cationic nanohydrogels as safe transport vehicles for pharmaceutical application of siRNA therapeutics.

METHODS

Unless otherwise indicated, all chemicals and solvents were commercially available and used as received unless otherwise indicated. Oregon Green 488 cadaverine was obtained from Invitrogen. Pentafluorophenol was obtained from Fluorochem (Great Britain, U.K.). Anhydrous dimethyl formamide (DMF) and dimethyl sulfoxide (DMSO) were obtained from Sigma-Aldrich and stored over activated molecular sieves (4 Å).

2,2′-Azobis(isobutyronitrile) (AIBN) was recrystallized from diethyl ether and stored at −7 °C. Anhydrous THF and dioxane were freshly distilled from a sodium/potassium mixture, anhydrous dichloromethane from calcium chloride. Phosphate buffered saline (PBS) was obtained from Fisher BioReagents containing 137 mM NaCl, 11.9 mM phosphates, and 2.7 mM KCl. Sodium acetate (NaOAc) buffer was prepared as 150 mM NaCl and 1.5 mM sodium acetate in Millipore water, and its pH was adjusted to 4.5. Column chromatography was done using silica obtained from Macharey-Nagel (0.063−0.2 mm/20−230 mesh). Dialysis was performed using Spectra/Por 3 membranes obtained from Carl Roth GmbH+Co.KG (Germany) with molecular weight cutoff of 8000−10 000 g/mol. Fluorescently labeled siRNA (Atto590) was purchased form IBA GmbH (Göttingen, Germany). Their sequence is directed against enhanced fluorescent protein (EGFP) (GenBank Accesion #U55762).

Sense strand: 5′-GCAAGCUGACCCUGAAGUUCAU-3′.

Anti sense strand: 3′-GCCGUUCGACUGGGACUUCAAG-5′.

The fluorescent dye Atto590 was covalently attached to the 3′-end of the sense strand. The siRNA duplexes were formed by mixing labeled sense and unlabeled antisense strands in PBS and incubating for 2 min at 95 °C followed by 1 h hybridization period at 37 °C.

Instrumentation. All ^{1}H and ^{13}C NMR spectra were recorded on a Bruker 300 MHz FT NMR spectrometer. All ^{19}F NMR spectra were recorded on a Bruker 400 MHz FT NMR spectrometer. Chemical shifts (δ) are given in parts per million relative to TMS. Samples were prepared in deuterated solvents and their signals referenced to residual nondeuterated solvent signals. The polymers' molecular weight was determined by gel permeation chromatography (GPC) in tetrahydrofuran (THF) as solvent and with the following parts: pump PU 1580, auto sampler AS1555, UV detector UV 1575 (detection at 254 nm), RI detector RI 1530 from JASCO. Columns were used from MZ-Analysentechnik: MZ-Gel SDplus 10^{2} Å and MZ-Gel SDplus 10^{6} Å. Calibration was done using polystyrene standards purchased from Polymer Standard Services. IR spectra were recorded on Perkin-Elmer 100 FTIR spectrometer using an ATR unit. ESI-MS was performed using a Navigator Instrument from Thermoelectronics with sample concentrations of 0.1 mg/mL, 0.75 mL/min flow rate, cone voltage 70, 45, or 35 V, and nitrogen flow rate 300 L/min. UV−vis spectra were recorded using a Jasco V-630 spectrophotometer (1 cm × 1 cm quartz cell). Fluorescence emission spectra were recorded using a Perkin luminescence spectrometer LS50B spectrofluorometer (right angle geometry, 1 cm × 1 cm quartz cell).

Syntheses. The syntheses of pentafluorophenyl methacrylate (PFPMA),[46] tri(ethylene glycol) methyl ether methacrylate (MEO_3MA),[52] 4-cyano-4-(phenylcarbonothioylthio) pentanoic acid,[56] and methoxy triethylene glycol amine[77,78] are described in detail in the Supporting Information.

Synthesis of Poly(pentafluorophenyl methacrylate) P(PFPMA). All P(PFPMA) polymers presented in this work were synthesized by RAFT polymerization as previously reported.[46,48] For a typical polymerization, a Schlenk tube equipped with a stir bar was loaded with pentafluorphenyl methacrylate (PFPMA) (4.00 g; 15.83 mmol), 4-cyano-4-(phenylcarbonothioylthio)pentanoic acid (111 mg; 0.40 mmol), and AIBN (6.5 mg; 0.04 mmol). All compounds were dissolved in anhydrous dioxane (4 mL). Following three freeze−pump−thaw cycles, the tube was immersed in an oil bath at 65 °C for about 17 h under vigorous stirring. The resulting polymer was isolated by precipitation in hexane and centrifugation. After redissolving in a few milliliters of dioxane, this process was repeated three times. The precipitated polymer was dried for 12 h at 40 °C under 10 mbar vacuum affording $P(PFPMA)_{46}$ (2.64 g; 64%) as a slightly red powder. GCP: M_n = 11800 g/mol; M_w = 14800 g/mol; PDI = 1.24. ^{1}H NMR ($CDCl_3$, 300 MHz): δ [ppm] = 2.80−2.10 (br, 2H, −CH_2−) and 1.80−1.00 (br, 3H, −CH_3). ^{13}C NMR ($CDCl_3$, 75 MHz): δ [ppm] = 172.90 (−CO_2−); 143.50−141.29 (o-ArC); 139.92−139.16 (p-ArC); 136.30 − 135.23 (m-ArC); 124.72 (ArC-O); 52.55 ($C_{quat.}$ polymer main chain); 46.05 (−CH_2− polymer main chain); 18.25 (−CH_3 polymer main chain). ^{19}F NMR ($CDCl_3$, 376 MHz): δ [ppm] = −150.31 to −151.39 (br, 2F, o-ArF); −156.91 (br, 1F, p-ArF); −162.05 (br, 2F, m-ArF).

Synthesis of Poly(tri(ethylene glycol)methyl ether methacrylate) P(MEO_3MA). All P(MEO_3MA) polymers presented in this work were synthesized by RAFT polymerization. For a typical polymerization, a Schlenk tube equipped with a stir bar was loaded with tri(ethylene glycol)methyl ether methacrylate (MEO_3MA) (2.00 g; 8.61 mmol), 4-cyano-4-(phenylcarbonothioylthio)pentanoic acid (30 mg; 0.11 mmol), and AIBN (2.3 mg; 0.01 mmol). All compounds were dissolved in anhydrous dioxane (3 mL). Following three freeze−pump−thaw cycles, the tube was immersed in an oil bath at 65 °C for about 14 h under vigorously stirring. The resulting polymer was isolated by precipitation in hexane and centrifugation. After redissolving in a few milliliters of dioxane, this process was repeated three times. The precipitated polymer was dried for 12 h at 40 °C under 10 mbar vacuum affording $P(MEO_3MA)_{44}$ (1.32 g; 66%) as a red oil. GCP: M_n = 10600 g/mol; M_w = 12400 g/mol; PDI = 1.17. ^{1}H NMR ($CDCl_3$, 300 MHz): δ [ppm] = 4.08 (br, 2H, COO−CH_2-CH_2−); 3.69 − 3.54 (br, 10H, COO−CH_2−CH_2−O-CH_2−CH_2−O−CH_2−CH_2−O−CH_3); 3.38 (br, 3H, O−CH_3); 2.10−1.60 (br, 2H, −CH_2− polymer main chain); 1.30−0.80 (br, 3H, −CH_3 polymer main chain). ^{13}C NMR ($CDCl_3$, 75 MHz): δ [ppm] = 177,13 (−CO_2−); 71.89 (CH_2−CH_2−O−CH_3); 70.58 (br, O−CH_2−CH_2−O−CH_2−CH_2−O−CH_3); 68.41 (COO−CH_2−CH_2−); 63.80 (COO−CH_2−CH_2−); 58.97 (O−CH_3); 54.07 ($C_{quat.}$ polymer main chain); 44.67 (−CH_2− polymer main chain); 18.51 (−CH_3 polymer main chain).

Block Copolymer Synthesis of Poly(pentafluorophenyl methacrylate)-*block*-Poly(tri(ethylene glycol)methyl ether methacrylate) P(PFPMA)-*b*-P(MEO_3MA). All P(PFPMA)-*b*-P(MEO_3MA) block copolymers presented in this work were synthesized by RAFT polymerization using previously synthesized P(PFPMA) homopolymers as macrochain transfer agents. For a typical polymerization, a Schlenk tube equipped with a stir bar was loaded with $P(PFPMA)_{61}$ (500 mg; 0.033 mmol), tri(ethylene glycol)methyl ether methacrylate (MEO_3MA) (0.77 g; 3.333 mmol), and AIBN (0.5 mg; 0.003 mmol). All compounds were dissolved in anhydrous dioxane (3 mL). Following three freeze−pump−thaw cycles, the tube was immersed in an oil bath at 65 °C for about 14 h under vigorous stirring. The resulting polymer was isolated by precipitation in hexane and centrifugation. After redissolving in a few milliliters of dioxane, this process was repeated three times. The precipitated polymer was dried for 12 h at 40 °C under 10 mbar vacuum affording $P(PFPMA)_{61}$-*b*-$P(MEO_3MA)_{26}$ (0.77 g; 62%) as a light red powder. GCP: M_n = 21600 g/mol; M_w = 25000 g/mol; PDI = 1.20. ^{1}H NMR ($CDCl_3$, 300 MHz): δ [ppm] = 4.09 (br, 2H, COO−CH_2−CH_2−); 3.69−3.54 (br, 10H, COO−CH_2−CH_2−O−CH_2−CH_2−O−CH_2−CH_2−O−CH_3); 3.39 (br, 3H, O−CH_3); 2.80−2.10 (br, 5H, −CH_2− PFPMA block main chain); 2.10−1.60 (br, 2H, −CH_2− MEO_3MA block main chain); 1.50−1.10 (br, 7H, −CH_3 PFPMA block main chain); 1.10−0.70 (br, 3H, −CH_3 MEO_3MA block main chain) (compare Supporting Information Figure S2). ^{13}C NMR ($CDCl_3$, 75 MHz): δ [ppm] = 177.21 (−CO_2− MEO_3MA); 172.45 (−CO_2− PFPMA); 142.84−141.49 (o-ArC); 139.92−139.16 (p-ArC); 137.84−135.56 (p-ArC); 124.72 (ArC−O); 71.91 (CH_2−CH_2−O−CH_3); 70.60 (br, O−CH_2−CH_2−O−CH_2−CH_2−O−CH_3); 68.45 (COO−CH_2−CH_2−); 63.85 (COO−CH_2−CH_2−); 59.00 (O−CH_3); 54.13 ($C_{quat.}$ MEO_3MA block main chain); 52.26 ($C_{quat.}$ PFPMA block main chain); 45.86 (−CH_2− PFPMA block main chain); 44.47 (−CH_2− MEO_3MA block main chain); 19,12 (−CH_3 PFPMA block main chain); 16.69 (−CH_3 MEO_3MA block main chain) (compare Supporting Information Figure S3). ^{19}F NMR ($CDCl_3$, 376 MHz): δ [ppm] = −150.27 to −151.33 (br, 2F, o-ArF); −156.86 (br, 1F, p-ArF); −162.02 (br, 2F, m-ArF) (compare Supporting Information Figure S4).

Block Copolymer Synthesis of Poly(tri(ethylene glycol)methyl ether methacrylate)-*block*-Poly(pentafluorophenyl methacrylate) P(MEO_3MA)-*b*-P(PFPMA). All P(MEO_3MA)-*b*-P(PFPMA) block copolymers presented in this work were synthesized by RAFT polymerization using previously synthesized P(MEO_3MA) homopolymers as macrochain transfer agents. For a typical polymerization, a Schlenk tube equipped with a stir bar was loaded with P-$(MEO_3MA)_{44}$ (450 mg; 0.042 mmol), pentafluorphenyl methacrylate (PFPMA) (0.45 g; 1.796 mmol), and AIBN (0.7 mg; 0.004 mmol). All compounds were dissolved in anhydrous dioxane (4 mL). Following three freeze−pump−thaw cycles, the tube was immersed in an oil bath at 65 °C for about 20 h under

vigorous stirring. The resulting polymer was isolated by precipitation in hexane and centrifugation. After redissolving in a few milliliters of dioxane, this process was repeated three times. The precipitated polymer was dried for 12 h at 40 °C under 10 mbar vacuum affording $P(MEO_3MA)_{44}$-*b*-$P(PFPMA)_8$ (0.51 g; 56%) as a light red oil. GCP: M_n = 12600 g/mol; M_w = 14600 g/mol; PDI = 1.16. ^{1}H NMR ($CDCl_3$, 300 MHz): δ [ppm] = 4.08 (br, 2H, COO−CH_2−CH_2−); 3.75−3.51 (br, 10H, COO−CH_2−CH_2−O−CH_2−CH_2−O−CH_2−CH_2−O−CH_3); 3.38 (br, 3H, O−CH_3); 2.70−2.20 (br, 0.3H, −CH_2− PFPMA block main chain); 2.20−1.60 (br, 2H, −CH_2− MEO_3MA block main chain); 1.60−1.10 (br, 0.45H, −CH_3 PFPMA block main chain); 1.10−0.60 (br, 3H, −CH_3 MEO_3MA block main chain) (compare Supporting Information Figure S2). ^{13}C NMR ($CDCl_3$, 75 MHz): δ [ppm] = 177.20 (−CO_2− MEO_3MA); 172.61 (−CO_2− PFPMA); 143.84−141.49 (o-Ar*C*); 139.92−139.16 (p-Ar*C*); 137.84−135.56 (m-Ar*C*); 124.72 (Ar*C*−O); 71.92 (CH_2−CH_2−O−CH_3); 70.53 (br, O−CH_2−CH_2−O−CH_2−CH_2−O−CH_3); 68.46 (COO−CH_2−CH_2−); 63.85 (COO−CH_2−CH_2−); 58.99 (O−CH_3); 54.55 ($C_{quat.}$ MEO_3MA block main chain); 52.26 ($C_{quat.}$ PFPMA block main chain); 45.86 (−CH_2− PFPMA block main chain); 44.45 (−CH_2− MEO_3MA block main chain); 18,61 (−CH_3 PFPMA block main chain); 16.68 (−CH_3 MEO_3MA block main chain) (compare Supporting Information Figure S3). ^{19}F NMR ($CDCl_3$, 376 MHz): δ [ppm] = −150.28 to −151.42 (br, 2F, o-Ar*F*); −156.79 (br, 1F, p-Ar*F*); −161.99 (br, 2F, m-Ar*F*) (compare Supporting Information Figure S4).

Removal of Dithiobenzoate End Groups. Dithiobenzoate end groups of polymers synthesized by RAFT polymerization can be removed according to a procedure reported by Perrier *et al.*[57] For a typical reaction, in Schlenk tube equipped with a stir bar, block copolymer $P(PFPMA)_{61}$-*b*-$P(MEO_3MA)_{26}$ (0.72 g; 0.033 mmol) and 4,4′-azo-bis(4-cyanovaleric acid) (ACVA) (0.29 g; 1.028 mmol; 30 times excess in relation to the polymer end group) were dissolved in 6 mL of anhydrous dioxane under nitrogen atmosphere. The reaction mixture was heated at 78 °C for 4 h while stirring vigorously. After the polymer solution turned colorless, the polymer was isolated by precipitation in a 1:1 mixture of hexane/diethyl ether and centrifuging. After redissolving in a few milliliters of dioxane, this process was repeated three times. The precipitated polymer was dried for 12 h at 40 °C under 10 mbar vacuum affording $P(PFPMA)_{61}$-*b*-$P(MEO_3MA)_{26}$ (0.72 g; quantitatively) as a colorless powder. The absence of the dithiobenzoate group was confirmed by UV−vis spectroscopy (compare Supporting Information Figure S1; absorption maxima at 310 and 500 nm disappear).

Synthesis of Cationic Nanohydrogel Particles. All nanohydrogel particles presented in this work were synthesized under similar conditions according to Table 4. For a typical reaction, in a round-bottom flask equipped with a stir bar, $P(PFPMA)_{61}$-*b*-$P(MEO_3MA)_{26}$ (51.9 mg; 2.40 μmol polymer or 147 μmol reactive ester) was dispersed in anhydrous DMSO (5.2 mL) under nitrogen atmosphere supported by sonication for 1 h. Oregon Green cadaverine (26.7 μL of a 2.5 mg/mL solution in DMSO; 0.14 μmol) was added first, followed by triethylamine (112 μL; 808 μmol) and spermine (136 μL of a 0.1 g/mL solution in DMSO; 67 μmol). The flask containing the reaction mixture was immersed in an oil bath at 50 °C under vigorous stirring, and ^{19}F NMR samples (0.1 mL dissolved in 0.5 mL of DMSO-d_6) were taken at certain time points to determine complete reactive ester conversion (compare Supporting Information Figure S7). After 16 h, no polymer-bound pentafluorophenol could be detected anymore. To remove further traces of it below the NMR detection limit, excess of non-cross-linking methoxy triethylene glycol amine (220 μL of a 0.1 g/mL solution in DMSO; 135 μmol) was added and the reaction mixture was stirred for an additional 20 h at 50 °C. To remove small molecular byproducts, the reaction mixture was afterward purified by dialysis against Millipore water for 2 days (including frequent water exchange) and subsequent lyophilization affording **NP1*** (31.0 mg, 79%) as an orange powder.

Pyrene Fluorescence Spectroscopy (refs 62−64). Stock solutions of $P(PFPMA)_{61}$-*b*-$P(MEO_3MA)_{26}$ or $P(MEO_3MA)_{44}$-*b*-$P(PFPMA)_8$ were prepared at a concentration of 1 mg/mL by dissolving in DMSO supported by sonication for 1 h. The polymer stock solution was then diluted to 10 different concentrations down to 1×10^{-5} mg/mL using further DMSO. Each sample was prepared by dropping carefully 60 μL of a pyrene (Aldrich, 98%) solution (2.5×10^{-5} mol/L in acetone) into 5 mL glass vials and evaporating the solvent overnight. On the next day, 3 mL of one of the polymer−DMSO solutions was added, affording pyrene solutions of 5.0×10^{-7} mol/L. The mixtures were incubated for 48 h at room temperature with shaking. Steady-state fluorescence spectra of the air-equilibrated samples were recorded using a Perkin luminescence spectrometer LS50B spectrofluorometer (right angle geometry, 1 cm × 1 cm quartz cell) using the following conditions: excitation at 333 ± 3 nm, detected emission spectrum from 350 to 460 nm. The intensities of pyrene's first and third vibronic band at 373.5 and 384.5 nm in DMSO were evaluated, and their ratio was plotted *versus* logarithmic polymer concentration. Linear extrapolations of steady ratio and decrease of ratio were done, and their intercept was determined as critical aggregation concentration (CAC).

Dynamic Light Scattering (DLS) Experiments of Block Copolymers and Nanohydrogel Particles. All block copolymer solutions in THF or DMSO as well as nanohydrogel particle solutions in PBS or NaOAc buffer were prepared at the concentrations as described. Cylindrical quartz cuvettes (20 mm diameter, Hellma, Mühlheim, Germany) were cleaned by dust-free distilled acetone and transferred into a dust-free flow box. Polymer solutions were filtered into these cuvettes through Millex LCR filters, 0.45 μm pore size (Millipore), for PBS solutions and through Millex LG filters, 0.22 μm pore size (Millipore), for THF or DMSO solutions. Then, dynamic light scattering (DLS) measurements were performed with an ALV-SP125 goniometer equipped with single-photon detector SO-SIPD, an ALV-5000 Multiple-Tau digital correlator, and a Spectra Physics 2060 argon ion laser (500 mW output at 514.5 nm wavelength). The scattered intensity was divided by a beam splitter (approximately 50:50), and each of the portions was detected by the photomultiplier. The two signals were cross-correlated to eliminate nonrandom electronic noise. All samples were typically measured from 30 to 150° in steps of 15°. Data evaluation was done according to literature:[79−81] all correlation functions usually showed monomodal decay and were fitted by a sum of two exponentials, from which the first cumulant Γ was calculated resulting in an angle-dependent diffusion coefficient D or reciprocal hydrodynamic radius R_h^{-1}, according to formal application of Stokes−Einstein law. By extrapolation of R_h^{-1}/q^2 to q = 0 z-average hydrodynamic radius $R_h = \langle R_h^{-1}\rangle_Z^{-1}$ was obtained. Dispersities were estimated by applying the cumulant method for each correlation function at 90°, resulting in μ_2 values of $\mu_2 = \Gamma_2/\Gamma_1^2$. Assuming spherical particles with a Gaussian distribution of radii, the normalized second cumulant μ_2 = 0.05 relates to a standard deviation σ_D = 0.22 of the diffusion coefficient, equivalent to a polydispersity in radius of roughly 25%. A value of μ_2 = 0.10 corresponds to a σ_D = 0.32 for the diffusion coefficient or to a polydispersity in radius of 50%. Therefore, values of μ_2 around 0.05 characterize samples with narrow size distributions. Values of μ_2 above 0.1, however, characterize very broadly distributed samples.

Fluorescence Correlation Spectroscopy (FCS) Experiments of Fluorescent Labeled Nanohydrogels and SiRNA. Fluorescence correlation spectroscopy (FCS) was performed using a commercial FCS setup (Zeiss, Germany) consisting of the module ConfoCor2 and an inverted microscope model Axiovert 200 with a Zeiss C-Apochromat 40×/1.2 W water immersion objective. As for the nanohydrogel particles, the fluorophores were excited by an argon laser (488 nm) and the emission was collected after filtering by a LP505 long pass filter. As for siRNA, however, the fluorophores were excited by a helium−neon laser (543 nm), and the emission was collected after filtering by a LP585 long pass filter. For detection, an avalanche photodiode that enables single-photon counting was used. An eight-well polystyrene chambered cover glass (Laboratory-Tek, Nalge Nunc International) was used as the sample cell. All nanohydrogel and siRNA solutions in PBS were prepared at the concentrations as described and transferred into the polystyrene chambers. For each sample, 10 measurements with a total duration of 5 min were performed. The time-dependent fluctuations of the fluorescent intensities $\delta I(t)$ were recorded and analyzed by an autocorrelation function $G(\tau) = 1 + \langle \delta I(t')\delta I(t' + \tau)\rangle / \langle \delta I(t')\rangle^2$. As it has been

shown theoretically for an ensemble of m different types of freely diffusing fluorescence species, $G(\tau)$ has the analytical form of[82]

$$G(\tau) = 1 + [1 + \frac{f_T}{1 - f_T} e^{-\tau/\tau_T}] \frac{1}{N} \sum_{i=1}^{m} \frac{f_i}{[1 + \frac{\tau}{\tau_{D,i}}] \sqrt{1 + \frac{\tau}{S^2 \tau_{D,i}}}}$$

Here, N is the average number of diffusing fluorescence species in the observation volume, f_T and τ_T are the fraction and the decay time of the triplet state, $\tau_{D,i}$ is the diffusion time of the ith species, f_i is the fraction of component i and S is the so-called structure parameter $S = z_0/r_0$, where z_0 and r_0 represent the axial and the radial dimensions of the confocal volume, respectively. Furthermore, the diffusion time $\tau_{D,i}$ is related to the respective diffusion coefficient D_i through $D_i = r_0^2/4\tau_{D,i}$. The experimental $G(\tau)$ was fitted yielding the corresponding diffusion times and, subsequently, the diffusion coefficient of the fluorescent species. According to the Stokes–Einstein law, the hydrodynamic radii R_h can be calculated assuming spherical particles. As the value of r_0 strongly depends on the specific characteristics of the optical setup, a calibration was performed using a reference standard with known diffusion coefficient, that is Rhodamine 6G.

Atomic Force Microscopy of Nanohydrogel Particles. All AFM imaging was conducted on a MFP-3-D-SA (Asylum Research, Santa Barbara, CA, USA) by constant amplitude tapping mode (intermittent contact mode) in air using a silicon cantilever (thickness = 4.6 μm, resonance frequency = 311.8–339.5 kHz, spring constant = 47.6–61.8 N/m, Olympus Atomic Forces, Mannheim, Germany). Nanohydrogel particles were usually prepared at 1 mg/mL in Millipore water, and 20 μL of each sample was dripped on even mica. Solvent was removed in vacuum at 10 mbar and 40 °C for 12 h before imaging. Therefore, the AFM probe was housed within a vibration-resistant case on a vibration isolation platform. Each sample was imaged at least three times at different locations on the substrate to ensure reproducibility. Each AFM image presented here consists of 512 scan lines for each direction.

Agarose Gel Electrophoresis. Atto590-labeled siRNA, the nanohydrogel particle, and the mixtures of both in PBS were prepared at concentrations as described. All samples incubated were incubated for 30 min. Loading buffer was added, and samples were transferred on a 0.5% agarose gel. Electrophoresis was performed at 90 V for 50 min, and upon excitation at 365 nm, fluorescence was imaged with a conventional digital camera.

Cell Uptake Studies. We used RBE4 cells (rat brain endothelial cells) grown in a 1:1 mixture of DMEM/Ham's-F10 medium containing 10% v/v FCS, 100 μg/mL Pen/Strep, and 1 ng/mL bFGF (all Invitrogen). Cells were incubated at standard growth conditions at 37 °C, high humidity, and 5% CO_2. All prepared buffers and solutions for the cell culture experiments (except for the nanohydrogel solutions and siRNA) were autoclaved or sterile filtered with 0.2 μm pore size cellulose filters. Then, 80 000 cells were seeded into 12-well plates on collagen-coated coverslips (3 μg/cm^2) 24 h before the experiment.

As negative control, 30 pmol of siRNA duplexes was diluted to a final 130 μL with Opti-MEM (Invitrogen). As reference, a control with cationic lipids was performed, using the standard transfection reagent Oligofectamine (Invitrogen). Next, 30 pmol siRNA was diluted to a final 100 μL of Opti-MEM and combined with a 30 μL mixture containing 6 μL of Oligofectamine diluted in Opti-Mem. For delivery of nanohydrogel particles or particles loaded with siRNA, 30 pmol of siRNA duplexes (0.42 μg) and 10.5 μg of nanohydrogel particles were diluted to a final volume of 40 μL with Opti-MEM (resulting in a weight to weight ratio of siRNA/nanohydrogel particles of 1:25). For complex formation, all samples were incubated for 20 min.

Before the samples were added dropwise to RBE4 cells, the medium was replaced with transfection medium (medium without FCS or antibiotics), resulting in a final culture volume of 750 μL. All cells were incubated at 37 °C until fixation. For fixation, cells were washed once with PBS and fixated for 10 min in PBS containing 4% formaldehyde. After two further PBS washing steps, the nuclei were stained with 500 μL of 1 μg/mL DAPI (4′,6-diamidino-2-phenylindole, Sigma-Aldrich) in PBS for 5 min. After another two PBS washing steps, the cover slides were finally rinsed with distilled water and mounted with fluorescent mounting medium (DAKO) on microscope slides and stored at 4 °C ready for use.

Confocal Imaging. Fixed cell samples were imaged on an inverted confocal microscope TCS SP5 (Leica, Wetzlar, Germany) equipped with an oil-immersion objective (63× magnification; NA 1.4) and a laser set capable of 405 nm/488 nm/561 nm excitation. Images were recorded at 512 × 512 8-bit-pixel resolution with a pinhole of 130 μm and confocal plane depth of 1.0 μm, resulting in a total image size width and height of 246 μm × 246 μm. Stacks were recorded at 0.5 μm step width. DAPI emission was recorded between 440 and 470 nm, Oregon Green between 510 and 540 nm, and Atto590 between 605 and 635 nm.

Conflict of Interest: The authors declare no competing financial interest.

Acknowledgment. The authors would like to thank Daniel J. Siegwart, Matthias Barz, and Helmut Ringsdorf for their scientific advice. Support by the Microscopy Core Facility of the Institute of Molecular Biology (IMB), Mainz, is gratefully acknowledged, as well as Angelika Kühnle for providing us access to AFM instruments. Generally, this work was financially supported by SAMT and COMATT. Moreover, L.N. wants to thank the Fond der Chemischen Industrie and the Max Planck Graduate School for financial funding.

Supporting Information Available: Further details about the synthesis of the monomers, the chain transfer agent, methoxytriethylene glycol amine, and the removal of the dithiobenozate group from the polymers are given. The results of the homopolymerization of PFPMA and MEO_3MA are presented, too. Moreover, additional light scattering data of the influence of LiBr on the polymers in THF and DMSO, the influence of the molecular weight of the aggregated block copolymer, and the ionic strength of the buffer on the nanohydrogel particle's size, a kinetic study about the reactive ester conversion using ^{19}F NMR, the calculation of the N/P ratio for the systems, and fluorescence spectra of the labeled particles are given, as well. Additionally, fluorescent confocal z-stack images of the cellular uptake of the nanogels and images of the uptake of siRNA-loaded unlabeled nanohydrogel particles were added. This material is available free of charge *via* the Internet at http://pubs.acs.org.

REFERENCES AND NOTES

1. Petros, R. A.; DeSimone, J. M. Strategies in the Design of Nanoparticles for Therapeutic Applications. *Nat. Rev. Drug Discovery* **2010**, *9*, 615–627.
2. Kabanov, A. V.; Vinogradov, S. V. Nanogels as Pharmaceutical Carriers: Finite Networks of Infinite Capabilities. *Angew. Chem., Int. Ed.* **2009**, *48*, 5418–5429.
3. Hamidi, M.; Azadi, A.; Rafiei, P. Hydrogel Nanoparticles in Drug Delivery. *Adv. Drug Delivery Rev.* **2008**, *60*, 1638–1649.
4. Oishi, M.; Nagasaki, Y. Stimuli-Responsive Smart Nanogels for Cancer Diagnostics and Therapy. *Nanomedicine* **2010**, *5*, 451–468.
5. Oh, J. K.; Siegwart, D. J.; Matyjaszewski, K. Synthesis and Biodegradation of Nanogels as Delivery Carriers for Carbohydrate Drugs. *Biomacromolecules* **2007**, *8*, 3326–3331.
6. Siegwart, D. J.; Srinivasan, A.; Bencherif, S. A.; Karunanidhi, A.; Oh, J. K.; Vaidya, S.; Jin, R.; Hollinger, J. O.; Matyjaszewski, K. Cellular Uptake of Functional Nanogels Prepared by Inverse Miniemulsion ATRP with Encapsulated Proteins, Carbohydrates, and Gold Nanoparticles. *Biomacromolecules* **2009**, *10*, 2300–2309.
7. Tamura, A.; Oishi, M.; Nagasaki, Y. Enhanced Cytoplasmic Delivery of siRNA Using a Stabilized Polyion Complex Based on PEGylated Nanogels with a Cross-Linked Polyamine Structure. *Biomacromolecules* **2009**, *10*, 1818–1827.
8. Tamura, A.; Oishi, M.; Nagasaki, Y. Efficient siRNA Delivery Based on PEGylated and Partially Quaternized Polyamine Nanogels: Enhanced Gene Silencing Activity by the Cooperative Effect of Tertiary and Quaternary Amino Groups in the Core. *J. Controlled Release* **2010**, *146*, 378–387.

9. Blackburn, W. H.; Dickerson, E. B.; Smith, M. H.; McDonald, J. F.; Lyon, L. A. Peptide-Functionalized Nanogels for Targeted siRNA Delivery. *Bioconjugate Chem.* **2009**, *20*, 960–968.
10. Fire, A.; Xu, S.; Montgomery, M. K.; Kostas, S. A.; Driver, S. E.; Mello, C. C. Potent and Specific Genetic Interference by Double-Stranded RNA in *Caenorhabditis elegans*. *Nature* **1998**, *391*, 806–811.
11. Elbashir, S. M.; Harborth, J.; Lendeckel, W.; Yalcin, A.; Weber, K.; Tuschl, T. Duplexes of 21-Nucleotide RNAs Mediate RNA Interference in Cultured Mammalian Cells. *Nature* **2001**, *411*, 494–498.
12. Dorsett, Y.; Tuschl, T. siRNAs: Applications in Functional Genomics and Potential as Therapeutics. *Nat. Rev. Drug Discovery* **2004**, *3*, 318–329.
13. Cejka, D.; Losert, D.; Wacheck, V. Short Interfering RNA (siRNA): Tool or Therapeutic? *Clin. Sci.* **2006**, *110*, 47–58.
14. Whitehead, K. A.; Langer, R.; Anderson, D. G. Knocking Down Barriers: Advances in siRNA Delivery. *Nat. Rev. Drug Discovery* **2009**, *8*, 129–138.
15. Dincer, S.; Turk, M.; Piskin, E. Intelligent Polymers as Nonviral Vectors. *Gene Ther.* **2006**, *12*, S139–S145.
16. Takahashi, Y.; Nishikawa, M.; Takakura, Y. Nonviral Vector-Mediated RNA Interference: Its Gene Silencing Characteristics and Important Factors To Achieve RNAi-Based Gene Therapy. *Adv. Drug Delivery Rev.* **2009**, *61*, 760–766.
17. Tseng, Y.-C.; Mozumdar, S.; Huang, L. Lipid-Based Systemic Delivery of siRNA. *Adv. Drug Delivery Rev.* **2009**, *61*, 721–731.
18. Akinc, A.; Zumbuehl, A.; Goldberg, M.; Leshchiner, E. S.; Busini, V.; Hossain, N.; Bacallado, S. A.; Nguyen; Langer, R.; Anderson, D. G. A Combinatorial Library of Lipid-like Materials for Delivery of RNAi Therapeutics. *Nat. Biotechnol.* **2008**, *26*, 561–569.
19. Love, K. T.; Mahon, K. P.; Levins, C. G.; Whitehead, K. A.; Querbes, W.; Dorkin, J. R.; Qin, J.; Akinc, A.; Langer, R.; Anderson, D. G.; *et al.* Lipid-like Materials for Low-Dose, *In Vivo* Gene Silencing. *Proc. Natl. Acad. Sci. U.S.A.* **2010**, *107*, 1864–1869.
20. Mahon, K. P.; Love, K. T.; Whitehead, K. A.; Qin, J.; Akinc, A.; Leshchiner, E.; Leshchiner, I.; Langer, R.; Anderson, D. G. Combinatorial Approach To Determine Functional Group Effects on Lipidoid-Mediated siRNA Delivery. *Bioconjugate Chem.* **2010**, *21*, 1448–1454.
21. Whitehead, K. A.; Sahay, G.; Li, G. Z.; Love, K. T.; Alabi, C. A.; Ma, M.; Zurenko, C.; Querbes, W.; Langer, R. S.; Anderson, D. G. Synergistic Silencing: Combinations of Lipid-like Materials for Efficacious siRNA Delivery. *Mol. Ther.* **2011**, *19*, 1688–1694.
22. Schroeder, A.; Levins, C. G.; Cortez, C.; Langer, R.; Anderson, D. G. Lipid-Based Nanotherapeutics for siRNA Delivery. *J. Intern. Med.* **2010**, *267*, 9–21.
23. Vaishnaw, A.; Gollob, J.; Gamba-Vitalo, C.; Hutabarat, R.; Sah, D.; Meyers, R.; de Fougerolles, T.; Maraganore, J. A Status Report on RNAi Therapeutics. *Silence* **2010**, *1*, 14.
24. Ringsdorf, H. Structure and Properties of Pharmacologically Active Polymers. *J. Polym. Sci., Part C: Polym. Symp.* **1975**, *51*, 135–153.
25. Gros, L.; Ringsdorf, H.; Schupp, H. Polymeric Antitumor Agents on a Molecular and on a Cellular Level? *Angew. Chem., Int. Ed. Engl.* **1981**, *20*, 305–325.
26. Smith, D.; Holley, A. C.; McCormick, C. L. RAFT-Synthesized Copolymers and Conjugates Designed for Therapeutic Delivery of siRNA. *Polym. Chem.* **2011**, *2*, 1428–1441.
27. Heredia, K. L.; Nguyen, T. H.; Chang, C.-W.; Bulmus, V.; Davis, T. P.; Maynard, H. D. Reversible siRNA–Polymer Conjugates by RAFT Polymerization. *Chem. Commun.* **2008**, 3245–3247.
28. York, A. W.; Huang, F.; McCormick, C. L. Rational Design of Targeted Cancer Therapeutics through the Multiconjugation of Folate and Cleavable siRNA to RAFT-Synthesized (HPMA-s-APMA) Copolymers. *Biomacromolecules* **2010**, *11*, 505–514.
29. Meyer, M.; Dohmen, C.; Philipp, A.; Kiener, D.; Maiwald, G.; Scheu, C.; Ogris, M.; Wagner, E. Synthesis and Biological Evaluation of a Bioresponsive and Endosomolytic siRNA–Polymer Conjugate. *Mol. Pharmaceutics* **2009**, *6*, 752–762.
30. Howard, K. A. Delivery of RNA Interference Therapeutics Using Polycation-Based Nanoparticles. *Adv. Drug Delivery Rev.* **2009**, *61*, 710–720.
31. Gaynor, J. W.; Campbell, B. J.; Cosstick, R. RNA Interference: A Chemist's Perspective. *Chem. Soc. Rev.* **2010**, *39*, 4169–4184.
32. Matsumoto, S.; Christie, R. J.; Nishiyama, N.; Miyata, K.; Ishii, A.; Oba, M.; Koyama, H.; Yamasaki, Y.; Kataoka, K. Environment-Responsive Block Copolymer Micelles with a Disulfide Cross-Linked Core for Enhanced siRNA Delivery. *Biomacromolecules* **2009**, *10*, 119–127.
33. Liu, Y.; Samsonova, O.; Sproat, B.; Merkel, O.; Kissel, T. Biophysical Characterization of Hyper-Branched Polyethylenimine-Graft-Polycaprolactone-Block-Mono-Methoxyl-Poly(ethylene glycol) Copolymers (hy-PEI-PCL-mPEG) for siRNA Delivery. *J. Controlled Release* **2011**, *153*, 262–268.
34. York, A. W.; Zhang, Y.; Holley, A. C.; Guo, Y.; Huang, F.; McCormick, C. L. Facile Synthesis of Multivalent Folate-Block Copolymer Conjugates *via* Aqueous RAFT Polymerization: Targeted Delivery of siRNA and Subsequent Gene Suppression. *Biomacromolecules* **2009**, *10*, 936–43.
35. Convertine, A. J.; Benoit, D. S. W.; Duvall, C. L.; Hoffman, A. S.; Stayton, P. S. Development of a Novel Endosomolytic Diblock Copolymer for siRNA Delivery. *J. Controlled Release* **2009**, *133*, 221–229.
36. Convertine, A. J.; Diab, C.; Prieve, M.; Paschal, A.; Hoffman, A. S.; Johnson, P. H.; Stayton, P. S. pH-Responsive Polymeric Micelle Carriers for siRNA Drugs. *Biomacromolecules* **2010**, *11*, 2904–2911.
37. Truong, N. P.; Jia, Z.; Burges, M.; McMillan, N. A. J.; Monteiro, M. J. Self-Catalyzed Degradation of Linear Cationic Poly (2-dimethylaminoethyl acrylate) in Water. *Biomacromolecules* **2011**, *12*, 1876–1882.
38. Truong, N. P.; Jia, Z.; Burgess, M.; Payne, L.; McMillan, N. A. J.; Monteiro, M. J. A Self-Catalyzed Degradable Cationic Polymer for Release of DNA. *Biomacromolecules* **2011**, *12*, 3540–3548.
39. Benoit, D. S. W.; Srinivasan, S.; Shubin, A. D.; Stayton, P. S. Synthesis of Folate-Functionalized RAFT Polymers for Targeted siRNA Delivery. *Biomacromolecules* **2011**, *12*, 2708–2714.
40. Davis, M. E.; Zuckerman, J. E.; Choi, C. H.; Seligson, D.; Tolcher, A.; Alabi, C. A.; Yen, Y.; Heidel, J. D.; Ribas, A. Evidence of RNAi in Humans from Systemically Administered siRNA *via* Targeted Nanoparticles. *Nature* **2010**, *464*, 1067–1070.
41. Gao, W.; Xiao, Z.; Radovic-Moreno, A.; Shi, J.; Langer, R.; Farokhzad, O. C. Progress in siRNA Delivery Using Multifunctional Nanoparticles. *Methods Mol. Biol.* **2010**, *629*, 53–67.
42. Gaspar, R.; Duncan, R. Polymeric Carriers: Preclinical Safety and the Regulatory Implications for Design and Development of Polymer Therapeutics. *Adv. Drug Delivery Rev.* **2009**, *61*, 1220–1231.
43. Siegwart, D. J.; Whitehead, K. A.; Nuhn, L.; Sahay, G.; Cheng, H.; Jiang, S.; Ma, M.; Lytton-Jean, A.; Langer, R.; Anderson, D. G.; *et al.* Combinatorial Synthesis of Chemically Diverse Core–Shell Nanoparticles for Intracellular Delivery. *Proc. Natl. Acad. Sci. U.S.A.* **2011**, *108*, 12996–13001.
44. Moad, G.; Rizzardo, E.; Thang, S. H. Living Radical Polymerization by the RAFT Process. *Aust. J. Chem.* **2005**, *58*, 379–410.
45. Moad, G.; Rizzardo, E.; Thang, S. H. Living Radical Polymerization by the RAFT Process—A Second Update. *Aust. J. Chem.* **2009**, *62*, 1402–1472.
46. Eberhardt, M.; Mruk, R.; Zentel, R.; Théato, P. Synthesis of Pentafluorophenyl(meth)acrylate Polymers: New Precursor Polymers for the Synthesis of Multifunctional Materials. *Eur. Polym. J.* **2005**, *41*, 1569–1575.
47. Gibson, M. I.; Fröhlich, E.; Klok, H.-A. Postpolymerization Modification of Poly(pentafluorophenyl Methacrylate): Synthesis of a Diverse Water-Soluble Polymer Library.

J. Polym. Sci., Part A: Polym. Chem. **2009**, *47*, 4332–4345.
48. Théato, P. Synthesis of Well-Defined Polymeric Activated Esters. *J. Polym. Sci., Part A: Polym. Chem.* **2008**, *46*, 6677–6687.
49. Barz, M.; Tarantola, M.; Fischer, K.; Schmidt, M.; Luxenhofer, R.; Janshoff, A.; Theato, P.; Zentel, R. From Defined Reactive Diblock Copolymers to Functional HPMA-Based Self-Assembled Nanoaggregates. *Biomacromolecules* **2008**, *9*, 3114–3118.
50. Barz, M.; Luxenhofer, R.; Zentel, R.; Kabanov, A. V. The Uptake of *N*-(2-Hydroxypropyl)-methacrylamide Based Homo, Random and Block Copolymers by Human Multi-Drug Resistant Breast Adenocarcinoma Cells. *Biomaterials* **2009**, *30*, 5682–5690.
51. Barz, M.; Canal, F.; Koynov, K.; Zentel, R.; Vicent, M. J. Synthesis and *In Vitro* Evaluation of Defined HPMA Folate Conjugates: Influence of Aggregation on Folate Receptor (FR) Mediated Cellular Uptake. *Biomacromolecules* **2010**, *13*, 2274–2282.
52. Han, S.; Hagiwara, M.; Ishizone, T. Synthesis of Thermally Sensitive Water-Soluble Polymethacrylates by Living Anionic Polymerizations of Oligo(ethylene glycol) Methyl Ether Methacrylates. *Macromolecules* **2003**, *36*, 8312–8319.
53. Lutz, J.-F. Polymerization of Oligo(ethylene glycol) (Meth)acrylates: Toward New Generations of Smart Biocompatible Materials. *J. Polym. Sci., Part A: Polym. Chem.* **2008**, *46*, 3459–3470.
54. Gao, W.; Liu, W.; Mackay, J. A.; Zalutsky, M. R.; Toone, E. J.; Chilkoti, A. *In Situ* Growth of a Stoichiometric PEG-like Conjugate at a Protein's N-Terminus with Significantly Improved Pharmacokinetics. *Proc. Natl. Acad. Sci. U.S.A.* **2009**, *106*, 15231–15236.
55. Webster, R.; Elliott, V.; Park, B. K.; Walker, D.; Hankin, M.; Taupin, P.; Veronese, F. M. PEG and PEG Conjugates Toxicity: Towards an Understanding of the Toxicity of PEG and Its Relevance to PEGylated Biologicals. In *PEGylated Protein Drugs: Basic Science and Clinical Applications*, Birkhäuser Basel: Berlin, 2009; pp 127–146.
56. Mitsukami, Y.; Donovan, M. S.; Lowe, A. B.; McCormick, C. L. Water-Soluble Polymers. 81. Direct Synthesis of Hydrophilic Styrenic-Based Homopolymers and Block Copolymers in Aqueous Solution *via* RAFT. *Macromolecules* **2001**, *34*, 2248–2256.
57. Perrier, S.; Takolpuckdee, P.; Mars, C. A. Reversible Addition–Fragmentation Chain Transfer Polymerization: End Group Modification for Functionalized Polymers and Chain Transfer Agent Recovery. *Macromolecules* **2005**, *38*, 2033–2036.
58. Roth, P. J.; Kessler, D.; Zentel, R.; Theato, P. A Method for Obtaining Defined End Groups of Polymethacrylates Prepared by the RAFT Process during Aminolysis. *Macromolecules* **2008**, *41*, 8316–8319.
59. Pissuwan, D.; Boyer, C.; Gunasekaran, K.; Davis, T. P.; Bulmus, V. *In Vitro* Cytotoxicity of RAFT Polymers. *Biomacromolecules* **2010**, *11*, 412–420.
60. Sawada, H. Architecture and Applications of Novel Self-Assembled Aggregates of Fluoroalkyl-End-Capped Oligomers. *J. Fluorine Chem.* **2000**, *101*, 315–324.
61. Sawada, H. Novel Self-Assembled Molecular Aggregates Formed by Fluoroalkyl End-Capped Oligomers and Their Application. *J. Fluorine Chem.* **2003**, *121*, 111–130.
62. Kalyanasundaram, K.; Thomas, J. K. Environmental Effects on Vibronic Band Intensities in Pyrene Monomer Fluorescence and Their Application in Studies of Micellar Systems. *J. Am. Chem. Soc.* **1977**, *99*, 2039–2044.
63. Wilhelm, M.; Zhao, C. L.; Wang, Y.; Xu, R.; Winnik, M. A.; Mura, J. L.; Riess, G.; Croucher, M. D. Poly(styrene-ethylene oxide) Block Copolymer Micelle Formation in Water: A Fluorescence Probe Study. *Macromolecules* **1991**, *24*, 1033–1040.
64. Colombani, O.; Ruppel, M.; Schubert, F.; Zettl, H.; Pergushov, D. V.; Müller, A. H. E. Synthesis of Poly(*n*-butyl acrylate)-block-Poly(acrylic acid) Diblock Copolymers by ATRP and Their Micellization in Water. *Macromolecules* **2007**, *40*, 4338–4350.
65. Zhang, L.; Eisenberg, A. Morphogenic Effect of Added Ions on Crew-Cut Aggregates of Polystyrene-*b*-poly(acrylic acid) Block Copolymers in Solutions. *Macromolecules* **1996**, *29*, 8805–8815.
66. Trappmann, B.; Ludwig, K.; Radowski, M. R.; Shukla, A.; Mohr, A.; Rehage, H.; Böttcher, C.; Haag, R. A New Family of Nonionic Dendritic Amphiphiles Displaying Unexpected Packing Parameters in Micellar Assemblies. *J. Am. Chem. Soc.* **2010**, *132*, 11119–11124.
67. Fluegel, S.; Buehler, J.; Fischer, K.; McDaniel, J. R.; Chilkoti, A.; Schmidt, M. Self-Assembly of Monodisperse Oligonucleotide–Elastin Block Copolymers into Stars and Compound Micelles. *Chem.—Eur. J.* **2011**, *17*, 5503–5506.
68. Urdiales, J. L.; Medina, M. A.; Sanchez-Jimenez, F. Polyamine Metabolism Revisited. *Eur. J. Gastroenterol. Hepatol.* **2001**, *13*, 1015–1019.
69. Xiong, X.-B.; Uludag, H.; Lavasanifar, A. Biodegradable Amphiphilic Poly(ethylene oxide)-Block-Polyesters with Grafted Polyamines as Supramolecular Nanocarriers for Efficient siRNA Delivery. *Biomaterials* **2009**, *30*, 242–253.
70. Xiong, X.-B.; Uludag, H.; Lavasanifar, A. Virus-Mimetic Polymeric Micelles for Targeted siRNA Delivery. *Biomaterials* **2010**, *31*, 5886–5893.
71. Shim, M. S.; Kwona, Y. J. Dual Mode Polyspermine with Tunable Degradability for Plasmid DNA and siRNA Delivery. *Biomaterials* **2011**, *32*, 4009–4020.
72. Nilles, K.; Theato, P. Sequential Conversion of Orthogonally Functionalized Diblock Copolymers Based on Pentafluorophenyl Esters. *J. Polym. Sci., Part A: Polym. Chem.* **2010**, *48*, 3683–3692.
73. Nilles, K.; Theato, P. Polymerization of an Activated Ester Monomer Based on 4-Vinylsulfonic Acid and Its Polymer Analogous Reaction. *Polym. Chem.* **2010**, *2*, 376–384.
74. Ellis, D. A.; Martin, J. W.; Muir, D. C. G.; Mabury, S. A. Development of an ^{19}F NMR Method for the Analysis of Fluorinated Acids in Environmental Water Samples. *Anal. Chem.* **2000**, *72*, 726–731.
75. Bencini, A.; Bianchi, A.; Enrique; Micheloni, M.; Ramirez, J. A. Proton Coordination by Polyamine Compounds in Aqueous Solution. *Coord. Chem. Rev.* **1999**, *188*, 97–156.
76. Behr, J.-P. The Proton Sponge: A Trick To Enter Cells the Viruses Did Not Exploit. *Chima* **1997**, *51*, 34–36.
77. Goncalves, M.; Estieu-Gionnet, K.; Berthelot, T.; Lain, G.; Bayle, M.; Canron, X.; Betz, N.; Bikfalvi, A.; Deleris, G. Design, Synthesis, and Evaluation of Original Carriers for Targeting Vascular Endothelial Growth Factor Receptor Interactions. *Pharm. Res.* **2005**, *22*, 1411–1421.
78. Dombi, K. L.; Griesang, N.; Richert, C. Oligonucleotide Arrays from Aldehyde-Bearing Glass with Coated Background. *Synthesis* **2002**, *2002*, 816–824.
79. Schmidt, M. Simultaneous Static and Dynamic Light Scattering: Application to Polymer Structure Analysis. In *Dynamic Light Scattering, The Method and Some Applications*; Brown, W., Ed.; Clarendon Press: Oxford, 1993.
80. Mueller, W.; Koynov, K.; Fischer, K.; Hartmann, S.; Pierrat, S.; Basché, T.; Maskos, M. Hydrophobic Shell Loading of PB-*b*-PEO Vesicles. *Macromolecules* **2008**, *42*, 357–361.
81. Mueller, W.; Koynov, K.; Pierrat, S.; Thiermann, R.; Fischer, K.; Maskos, M. pH-Change Protective PB-*b*-PEO Polymersomes. *Polymer* **2011**, *52*, 1263–1267.
82. Riegler, R.; Elson, E. S. *Fluorescence Correlation Spectroscopy*; Springer: New York, 2001.